The BEACH-containing protein WDR81 coordinates p62 and LC3C to promote aggrephagy

Xuezhao Liu,[1,2,3]* Yang Li,[1]* Xin Wang,[1,2,3] Ruxiao Xing,[1,5] Kai Liu,[1] Qiwen Gan,[1,5] Changyong Tang,[1,5] Zhiyang Gao,[1] Youli Jian,[1] Shouqing Luo,[4] Weixiang Guo,[1] and Chonglin Yang[1,2,3]

[1]State Key Laboratory of Molecular Developmental Biology, Institute of Genetics and Developmental Biology, Chinese Academy of Sciences, Beijing 100101, China
[2]State Key Laboratory for Conservation and Utilization of Bio-Resources in Yunnan and [3]Center for Life Sciences, School of Life Sciences, Yunnan University, Kunming 650091, China
[4]Peninsula Schools of Medicine and Dentistry, Institute of Translational and Stratified Medicine, Plymouth University, Plymouth PL6 8BU, England, UK
[5]Graduate School, University of Chinese Academy of Sciences, Beijing 100093, China

Autophagy-dependent clearance of ubiquitinated and aggregated proteins is critical to protein quality control, but the underlying mechanisms are not well understood. Here, we report the essential role of the BEACH (beige and Chediak–Higashi) and WD40 repeat-containing protein WDR81 in eliminating ubiquitinated proteins through autophagy. WDR81 associates with ubiquitin (Ub)-positive protein foci, and its loss causes accumulation of Ub proteins and the autophagy cargo receptor p62. WDR81 interacts with p62, facilitating recognition of Ub proteins by p62. Furthermore, WDR81 interacts with LC3C through canonical LC3-interacting regions in the BEACH domain, promoting LC3C recruitment to ubiquitinated proteins. Inactivation of LC3C or defective autophagy results in accumulation of Ub protein aggregates enriched for WDR81. In mice, WDR81 inactivation causes accumulation of p62 bodies in cortical and striatal neurons in the brain. These data suggest that WDR81 coordinates p62 and LC3C to facilitate autophagic removal of Ub proteins, and provide important insights into CAMRQ2 syndrome, a WDR81-related developmental disorder.

Introduction

Protein misfolding frequently occurs during the process of normal protein synthesis, and can be greatly exacerbated by cellular stresses such as heat shock, ER stress, and oxidative stress (Goldberg, 2003). If not properly resolved, misfolded proteins can further aggregate and impair cellular functions (Kopito, 2000; Kirkin et al., 2009b; Tyedmers et al., 2010). Clearance of aggregated protein is thus critical to cell homeostasis, defects in which are associated with many late-onset neurodegenerative disorders, including Parkinson's disease and Huntington's disease (Rubinsztein, 2006).

Autophagy can selectively remove ubiquitinated and aggregated proteins, thus serving as a protein quality-control system (Rubinsztein, 2006; Gamerdinger et al., 2009). Autophagic clearance of aggregated proteins, also termed "aggrephagy," requires the recognition of ubiquitinated and aggregated proteins by receptors such as p62/SQSTM1 and NBR1 (Noda et al., 2010; Johansen and Lamark, 2011). p62/SQSTM1 is a general cargo receptor that preferentially binds Ub chains linked by K63 through the C-terminal Ub-associated domain (Seibenhener et al., 2004; Komatsu et al., 2007; Pankiv et al., 2007; Rogov et al., 2014). In addition, p62 interacts with members of the LC3 and GABARAP subfamilies through an LC3-interacting region (LIR; Bjørkøy et al., 2005; Komatsu et al., 2007; Pankiv et al., 2007). Because p62 recognizes a diverse range of ubiquitinated cargos and interacts with LC3 or GABARAP family members in a nonselective manner, additional receptors or scaffold/adaptor proteins cooperate with p62 to promote selective autophagy (Johansen and Lamark, 2011; Rogov et al., 2014; Khaminets et al., 2016). For example, the Huntington's disease gene-encoded Huntingtin protein interacts with p62 and functions as a scaffold that recruits ULK1 but excludes mTOR, thus promoting selective autophagy of several cargos (Rui et al., 2015). ALFY/WDFY3, a PtdIns3P-binding protein, plays an important role in aggrephagy by interacting with p62 and Atg5-12 (Clausen et al., 2010; Filimonenko et al., 2010). In the nematode *Caenorhabditis elegans*, EPG-7 acts as a scaffold that interacts with the p62 homologue SQST-1 and a variety of autophagy regulators to mediate clearance of aggregated proteins in embryo development (Lin et al., 2013). The cargo specificity of autophagy may be achieved by selective interaction of certain p62-interacting

*X. Liu and Y. Li contributed equally to this paper.

Correspondence to Weixiang Guo: wxguo@genetics.ac.cn; Chonglin Yang: clyang@genetics.ac.cn

Abbreviations used: ANOVA, analysis of variance; BEACH, beige and Chediak–Higashi; BFA1, bafilomycin A1; cKO, conditional knockout; CLIR, candidate noncanonical LC3-interacting region; E, embryonic day; LIR, LC3-interacting region; MEF, mouse embryonic fibroblast; NRK, normal rat kidney; P, postnatal day; PI3K, phosphatidylinositol-3-kinase; TEM, transmission EM; Ub, ubiquitin.

The Rockefeller University Press $30.00
J. Cell Biol. Vol. 216 No. 5 1301–1320
https://doi.org/10.1083/jcb.201608039

scaffolds or receptors with members of the LC3 or GABARAP family. For instance, NDP52 selectively interacts with LC3C to mediate bacterial autophagy (von Muhlinen et al., 2012). In the aggrephagy pathway, ALFY was recently found to mainly interact with GABARAP (Lystad et al., 2014). In *C. elegans*, the LC3 homologues LGG-1 and LGG-2 bind to distinct groups of autophagy substrates, thus playing different roles in aggrephagy (Wu et al., 2015).

Although aggrephagy is critical to protein quality control, the mechanisms determining the selectivity of cargo recognition and autophagosome formation during aggrephagy are not fully understood. In this study, we identify WDR81, a BEACH (beige and Chediak–Higashi) domain– and WD40-containing protein, as an essential regulator of aggrephagy. WDR81 and its *C. elegans* homologue, SORF-2, were recently shown to function in maintaining endosomal PtdIns3P levels by forming a complex with another WD40-containing protein, WDR91 (Liu et al., 2016; Rapiteanu et al., 2016). Here, we uncover a distinct function of WDR81 in aggrephagy. We show that WDR81 directly interacts with p62 and promotes the recognition of ubiquitinated proteins. We further demonstrate that out of the three isoforms of the autophagosome membrane protein LC3, WDR81 preferentially interacts with LC3C to facilitate the removal of ubiquitinated proteins. We provide evidence that knocking out WDR81 results in accumulation of p62 bodies in mouse brain. These findings establish WDR81 as an essential regulator of aggrephagy and provide valuable insights into CAMRQ2 syndrome, a WDR81-related neuronal disorder.

Results

Inactivation of WDR81 causes accumulation of ubiquitinated and aggregated proteins

Previously, we found that WDR81 partially localizes to endosomes and forms a complex with WDR91 to regulate early-to-late endosome conversion (Liu et al., 2016). The fact that a substantial proportion of WDR81 is not located on endosomes suggests that WDR81 may have other functions in addition to a role in intracellular trafficking. To explore this possibility, we examined whether WDR81 localizes to the Golgi apparatus, ER, or mitochondria. Immunostaining revealed that WDR81 does not obviously colocalize with the Golgi protein GM130 or the ER protein Sec61β, suggesting that WDR81 does not act in the Golgi or ER (Fig. S1 A). Partial colocalization of WDR81 with MitoTracker Red staining was detected, as previously reported in mice (Fig. S1 A; Traka et al., 2013). Interestingly, we found that WDR81 substantially costained with ubiquitin in HeLa cells and human neuroblastoma SH-SY5Y cells (Fig. 1 A). To consolidate this observation, we treated HeLa cells with MG132, a proteasome inhibitor that induces accumulation of polyubiquitinated misfolded proteins (Kawaguchi et al., 2003; Salomons et al., 2009), or puromycin, a proteotoxin that induces premature release of polypeptide chains from ribosomes (Blobel, 1971). Both MG132 and puromycin induced formation of large Ub-positive focal structures that were enriched in WDR81 (Fig. 1 B). In contrast, tunicamycin or FCCP (carbonyl cyanide-4-(trifluoromethoxy)phenylhydrazone), which induces ER stress or depolarizes mitochondrial membrane potential, respectively, did not induce formation of WDR81-positive foci (Fig. S1 B). These results suggest that WDR81 likely participates in a process involving ubiquitinated and misfolded proteins. To investigate this possibility, we depleted WDR81 using siRNA or CRISPR/Cas9 (Fig. 1, C and D; Liu et al., 2016) and then examined the levels of Ub proteins. In HeLa cells and SH-SY5Y cells, WDR81 siRNA (si81) greatly increased the number and size of Ub protein foci compared with control siRNA (siCtrl; Fig. 1, E and F). Some of these Ub protein foci were also positive for p62/SQSTM1, a receptor for diverse autophagy cargoes (Fig. 1, E and F; Bjørkøy et al., 2005; Komatsu et al., 2007; Pankiv et al., 2007). Similarly, large Ub protein foci that costained with p62 were frequently observed in WDR81 knockout (KO-81) HeLa cells, but not control HeLa cells (Fig. 1 G). The levels of Ub proteins and p62, as revealed by immunoblotting, were strongly elevated in si81 or KO-81 cells (Fig. 1, H–J). The increased Ub proteins in KO-81 cells contained predominantly K63-linked Ub chains (K63-Ub), whereas the levels of Ub proteins with K48-linked Ub (K48-Ub) were not changed (Fig. 1 K). Consistent with this, the MG132- or puromycin-induced WDR81 foci were mainly positive for K63-Ub but only partially costained with K48-Ub (Fig. 1 L). In addition, we evaluated the effect of si81 on polyQ aggregates. In HeLa cells inducibly expressing Htt97Q-GFP, si81 significantly increased the number of polyQ foci, comparable to that caused by knocking down several major autophagy regulators, including the p62 receptor, the aggrephagy scaffold protein ALFY (Bjørkøy et al., 2005; Filimonenko et al., 2010), and the core autophagy factors Atg5 and Beclin1 (Fig. S2, A and B). Collectively, these findings suggest that WDR81 is important for preventing the accumulation of ubiquitinated and aggregated proteins.

WDR81 acts in the autophagy pathway for clearance of ubiquitinated and aggregated proteins

Given that proteins with K63-linked polyubiquitination are mainly degraded through autophagy (Newton et al., 2008; Tan et al., 2008; Kirkin et al., 2009b; Wong and Cuervo, 2010; Matsumoto et al., 2011; Rui et al., 2015), we investigated whether WDR81 promotes Ub protein clearance in an autophagy-dependent manner. Although si81 or KO-81 HeLa cells accumulated much higher levels of Ub proteins and p62 than cells with siCtrl, MG132 treatment further enhanced the levels of Ub proteins and p62 in these cells (Fig. 2, A and B). Because MG132 causes inhibition of the ubiquitin-proteasome system (Kawaguchi et al., 2003), the additive effect of si81 and MG132 suggests that WDR81 does not act in proteasome-dependent clearance of Ub proteins. Next, we knocked down WDR81 in both wild-type and *ATG5*$^{-/-}$ mouse embryonic fibroblast (MEF) cells (Kuma et al., 2004). As shown in Fig. 2 C, Ub proteins accumulated similarly in *ATG5*$^{-/-}$ MEF cells or si81 MEF cells; nevertheless, si81 treatment did not further enhance the levels of Ub proteins in *ATG5*$^{-/-}$ cells. Likewise, the elevation in p62 protein levels in *ATG5*$^{-/-}$ MEF cells was not enhanced with si81 treatment (Fig. 2 D). These results suggest that WDR81 acts through autophagy to promote clearance of Ub proteins. Consolidating this conclusion, we found that WDR81 and Ub proteins colocalized to large focal structures in *ATG5*$^{-/-}$ MEF cells, and the fluorescence intensities of endogenous WDR81 staining were significantly higher in *ATG5*$^{-/-}$ MEF cells and *ATG12*$^{-/-}$ normal rat kidney (NRK) cells (Figs. 2 E and S2 C). Furthermore, ectopically expressed BFP-WDR81 colocalized with Myc-Ub and the autophagosome-decorating GFP-LC3B to punctate

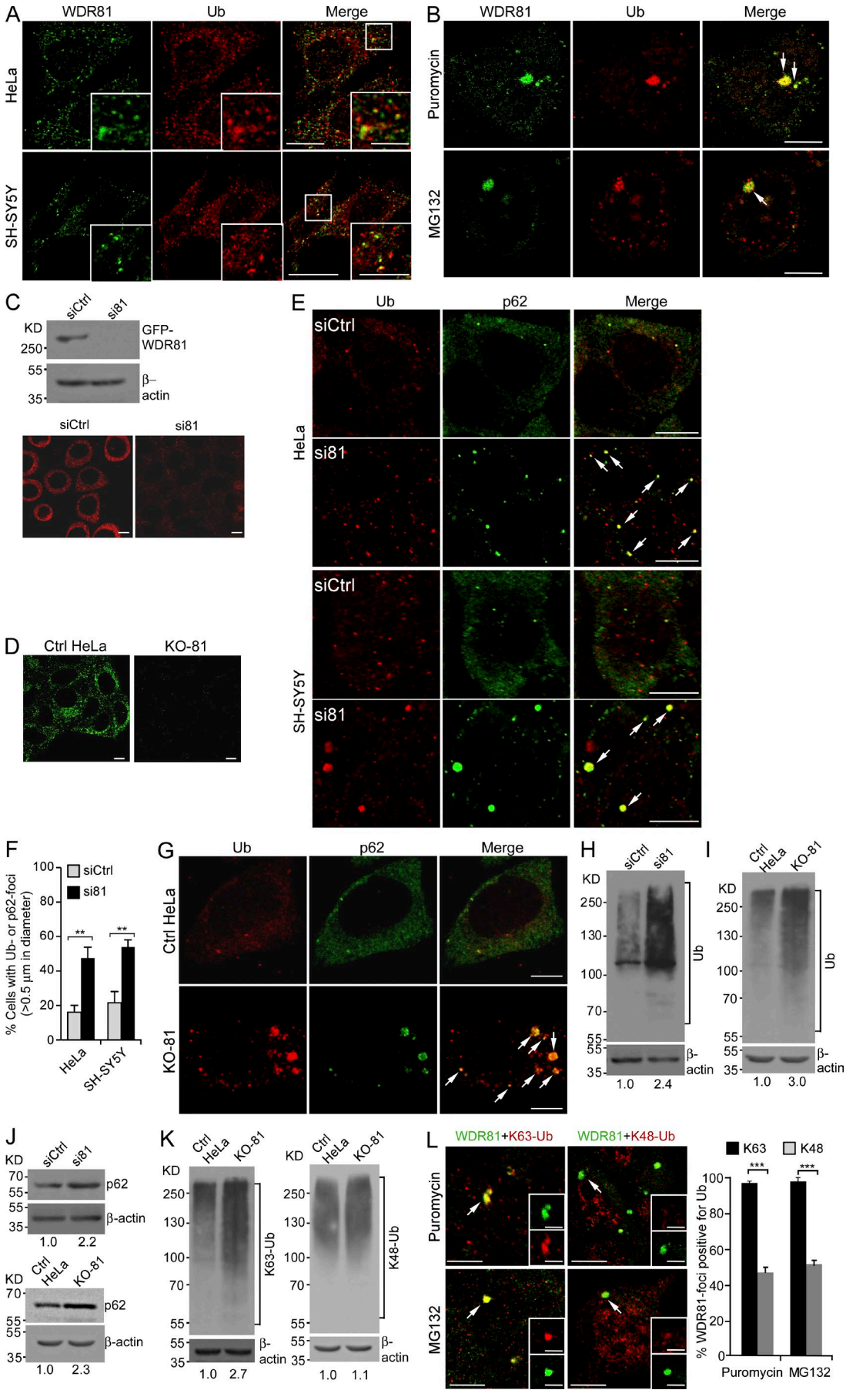

structures, which became even more obvious when cells were treated with MG132 (Fig. 2 F).

To investigate if WDR81 is degraded through autophagy, we knocked down the core components of the autophagy machinery or used bafilomycin A1 (BFA1) to inhibit lysosomal activity. siRNA of ATG5 or Beclin1 strongly increased Flag-WDR81 that was stably expressed in HeLa cells (Fig. 2 G). Levels of stably expressed Flag-WDR81 were similarly enhanced with BFA1 treatment (Fig. 2 H). These results suggest that WDR81 acts in autophagic clearance of Ub proteins and can be degraded through autophagy. Interestingly, MG132 treatment also enhanced Flag-WDR81 levels (Fig. 2 H), suggesting that the ubiquitin-proteasome system may contribute to WDR81 stability. In addition, we investigated whether WDR81 is required for general autophagy by examining the LC3 forms in KO-81 cells. The LC3-II/LC3-I ratio was the same in KO-81 and control cells (Fig. S2 D). Starvation (Earle's Balanced Salt Solution treatment) or lysosomal inhibition (BFA1) did not alter this ratio either (Fig. S2 D). Consistent with this, KO-81 cells did not show a significant increase in GFP-LC3 foci compared with control cells when cultured normally or treated with Earle's Balanced Salt Solution or BFA1 (Fig. S2 E). Using the RFP-GFP-LC3 fusion protein as an indicator, we found that the numbers of autophagosomes and autolysosomes were similar in control cells and KO-81 cells without or with starvation or BFA1 treatment (Fig. S2 F). Altogether, these findings suggest that WDR81 is unlikely to play a role in general autophagy.

The function of WDR81 in aggrephagy is independent of the endosomal WDR91–WDR81 complex

Because WDR81 and WDR91 form a complex to promote endosome maturation (Liu et al., 2016; Rapiteanu et al., 2016), we asked whether knockout of WDR91 also induced accumulation of Ub protein and p62 foci. Unlike KO-81 cells, WDR91 knockout (KO-91) cells do not contain enlarged foci of Ub proteins and p62 (Fig. S3 A). In addition, puromycin- or MG132-induced p62 foci were negative for WDR91 (Fig. S3 B). Given that inactivation of WDR81 or WDR91 similarly impairs endosome conversion (Liu et al., 2016; Rapiteanu et al., 2016), these results suggest that the elevation in Ub proteins and p62 in KO-81 cells do not result from defective endosome maturation. Supporting this conclusion, coexpression of GFP-WDR81 with mCherry-WDR91 (mCh-WDR91) led to perfect colocalization of these proteins with obvious endosomal structures, suggesting that WDR91 promotes the recruitment of WDR81 to endosomes (Fig. 3, A and B); however, MG132 or puromycin induced formation of distinct GFP-WDR81 foci separate from mCh-WDR91 (Fig. 3 A). Similarly, whereas GFP-WDR81 colocalized fairly well with the late endosome–specific marker Rab7 tagged with mCherry (mCh-Rab7), GFP-WDR81 no longer colocalized with mCh-Rab7 after MG132 or puromycin treatment (Fig. 3 B). In contrast, MG132 or puromycin did not change the colocalization of GFP-WDR91 with mCh-Rab7 (Fig. 3 C). These findings suggest that the function of WDR81 in aggrephagy is independent of the endosomal WDR81–WDR91 complex. In addition, whereas WDR81 and WDR91 form a complex with Beclin1 and their knockout enhanced Beclin1-dependent endosomal phosphatidylinositol-3-kinase (PI3K) activity (Liu et al., 2016; Fig. 3 D), neither protein was found in the Atg14L–Beclin1–Vps34 complex, and knockout of either WDR81 or WDR91 did not affect autophagic PI3K activity (Fig. 3 D). This suggests that WDR81 does not fulfill its role in aggrephagy by affecting autophagic PI3K activity.

To understand the requirement for WDR81 in aggrephagy, we performed transmission EM (TEM) analysis of control and KO-81 HeLa cells with MG132 treatment. The total number of autophagic vesicles (autophagosomes and autolysosomes) in control and KO-81 cells was not significantly different (Fig. 3, E and F), confirming that loss of WDR81 did not affect general autophagy. Remarkably, the autophagic vesicles in control cells predominantly contained darkly stained proteinaceous material and had intact membranes (Fig. 3, E and H). KO-81 cells, however, contained many proteinaceous structures in the cytosol that were more darkly stained and were either not enclosed by membranes or only partially surrounded by membranes (Fig. 3, E, G, and H). These results suggest that loss of WDR81 impaired the delivery or sequestration of aggregated proteins within autophagosomes.

WDR81 functions together with p62

To pinpoint how WDR81 functions in aggrephagy, we investigated whether it acts in complex with p62. In *ATG5*$^{-/-}$ MEF cells, WDR81 and p62 colocalized to large focal structures, suggesting that these two factors likely act at the same stage during aggrephagy (Fig. 4 A). Likewise, puromycin or MG132 treatment induced colocalization of WDR81 and p62 to large focal structures (Fig. S4 A). Because p62 overexpression results in formation of p62 bodies (Bjørkøy et al., 2005; Szeto et al., 2006; Pankiv et al., 2007; Clausen et al., 2010), we tested if such p62 bodies could recruit WDR81. As shown in Fig. 4 B, BFP-WDR81 coexpressed with GFP-p62 localized exclusively to p62 bodies. Likewise, overexpressed GFP-p62 recruited endogenous WDR81 to focal structures in both HeLa

Figure 1. **WDR81 inactivation causes accumulation of Ub proteins.** (A) Colocalization of endogenous WDR81 and Ub proteins in HeLa and SH-SY5Y cells. Insets show magnified (2×) views of the box in the merged images. (B) Colocalization of endogenous WDR81 and Ub proteins (arrows) to large focal structures in HeLa cells treated with 1 µg/ml puromycin or 10 µM MG132 for 12 h. Arrows indicate the enlarged foci costained with WDR81 and Ub. (C) WDR81 siRNA effectively knocks down WDR81. Left: HeLa cells stably expressing GFP-WDR81 were transfected with siRNA (siCtrl) or WDR81 siRNA (si81) oligos. Cells were subjected to Western blot analysis using GFP antibody 48 h after transfection. Right: HeLa cells were treated with siCtrl or siWDR81 and stained with WDR81 antibody 48 h after transfection. (D) Immunostaining of endogenous WDR81 in control and KO-81 HeLa cells. (E and F) Immunostaining (E) and quantification (F) of Ub protein and p62 foci in HeLa and SH-SY5Y cells treated with siCtrl or si81. Arrows indicate the enlarged foci costained with Ub and p62. (G) Immunostaining of Ub proteins and p62 in control and KO-81 HeLa cells. Arrows indicate the enlarged foci costained with Ub and p62. (H) Immunoblotting of Ub proteins in HeLa cells transfected with siCtrl or siWDR81. (I) Immunoblotting of Ub proteins in control or KO-81 HeLa cells. (J) Immunoblotting of p62 in siCtrl and si81 (top) or Ctrl and KO-81 cells (bottom). (K) Immunoblotting of K63-Ub or K48-Ub in control and KO-81 cells. (L) Colocalization of endogenous WDR81 with K63- or K48-linked Ub proteins (K63-Ub or K48-Ub) in HeLa cells treated with 1 µg/ml puromycin or 10 µM MG132 for 12 h. Insets show images of WDR81 foci (green) and K63-Ub or K48-Ub foci (red) indicated by arrows in the main panels. Quantification of Ub proteins and WDR81 is shown in the right panel. ≥40 WDR81 foci were examined for each Ub antibody. Bars: (all images) 10 µm; (insets) 5 µm. For all quantifications, data (mean ± SEM) were from three independent experiments and analyzed using ANOVA. **, P < 0.01; ***, P < 0.001. Fold changes of Ub proteins or p62 (H–K) were normalized to control and are indicated at the bottom.

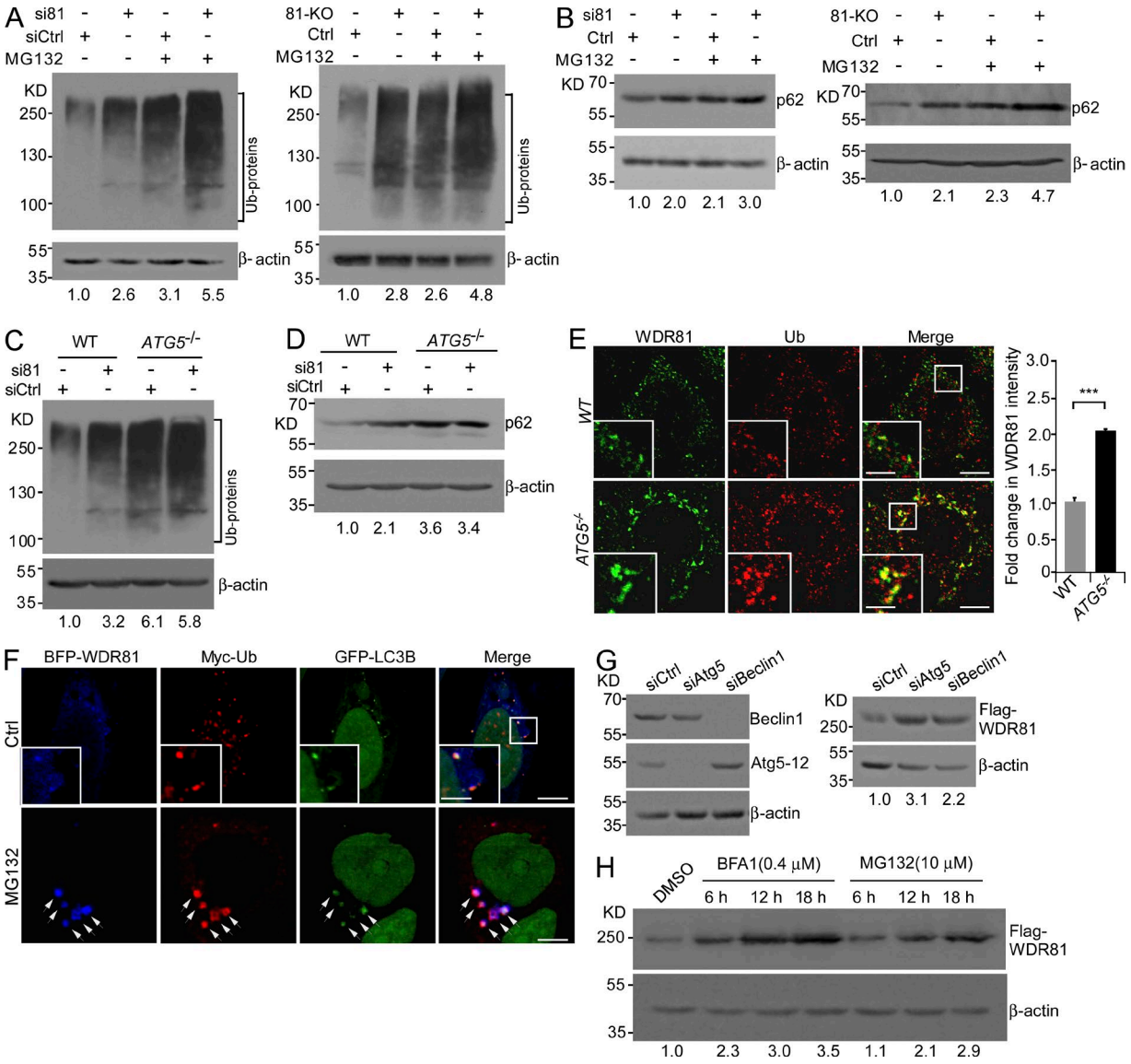

Figure 2. **WDR81 acts in the autophagy pathway for clearance of Ub proteins.** (A) Immunoblotting of Ub proteins in siCtrl or si81 (left) and control or KO-81 (right) HeLa cells treated without or with MG132. (B) Immunoblotting of p62 in siCtrl or siWDR81 (left) and control or KO-81 (right) HeLa cells treated without or with MG132. (C and D) Immunoblotting of Ub proteins (C) and p62 (D) in siCtrl- or si81-treated wild-type (WT) and *ATG5*$^{-/-}$ MEF cells. In A–D, fold changes of Ub proteins or p62 were normalized to control and are indicated at the bottom. (E) Immunostaining of WDR81 and Ub proteins in WT and *ATG5*$^{-/-}$ MEF cells. Insets in the bottom left corner show magnified (1.8×) views of the box in the merged images. Bars: (all images) 10 µm; (insets) 5 µm. Quantification of WDR81 intensity is shown in the right panel. Data (mean ± SEM) were from three independent experiments and analyzed using unpaired *t* tests. ***, $P < 0.001$. (F) Colocalization of BFP-WDR81, Myc-Ub and GFP-LC3B in HeLa cells treated without (Ctrl) or with MG132. In the Ctrl group, insets show magnified (1.8 x) views of the boxed region in the merged image. In the MG132 group, arrows indicate the large foci containing all three tagged proteins. Bars: (main images) 10 µm; (insets) 5 µm. (G) WDR81 is degraded by the autophagy pathway. HeLa cells stably expressing Flag-WDR81 were treated with siAtg5 or siBeclin1. Knockdown efficiency, determined by immunoblotting, is shown in the left panel. The siRNA-induced change in Flag-WDR81 levels is shown in the right panel. (H) Immunoblotting of Flag-WDR81 cells treated with 0.4 µM BFA1 and 10 µM MG132 for the indicated times. In G and H, fold changes of Flag-WDR81 were normalized to control and are indicated at the bottom. The treatment of cells with puromycin or MG132 was performed as in Fig. 1 (except in H).

and SH-SY5Y cells (Figs. 4 B and S4 B). GFP-tagged NBR1 (GFP-NBR1), a p62-like cargo receptor (Kirkin et al., 2009a), also formed obvious foci when overexpressed. Nevertheless, these GFP-NBR1 foci failed to recruit either ectopically expressed mCh-WDR81 or endogenous WDR81 (Fig. S4 C). In addition, mCherry-tagged NDP52, optineurin, and TAX1BP1, which are adaptors for xenophagy or mitophagy (Wild et al., 2011; von Muhlinen et al., 2012; Lazarou et al., 2015), localized to large Myc-Ub–positive focal structures in cells treated with MG132 (Fig. S4 D). However, they did not colocalize with GFP-WDR81 to focal structures in cells without MG132 treatment (Fig. S4 E). Together, these findings suggest that WDR81 is preferentially recruited by p62. In addition, colocalization of BFP-WDR81 with EGFP-p62 and mCh-WDR91 was observed in cells coexpressing these three proteins; however, WDR91 did not localize to p62 bodies (Fig. 4 C), suggesting that WDR81 plays dual roles in aggrephagy and endosome conversion by acting with p62 and WDR91, respectively.

We next attempted to identify the region in WDR81 that mediates colocalization with p62. By coexpressing mCh-p62

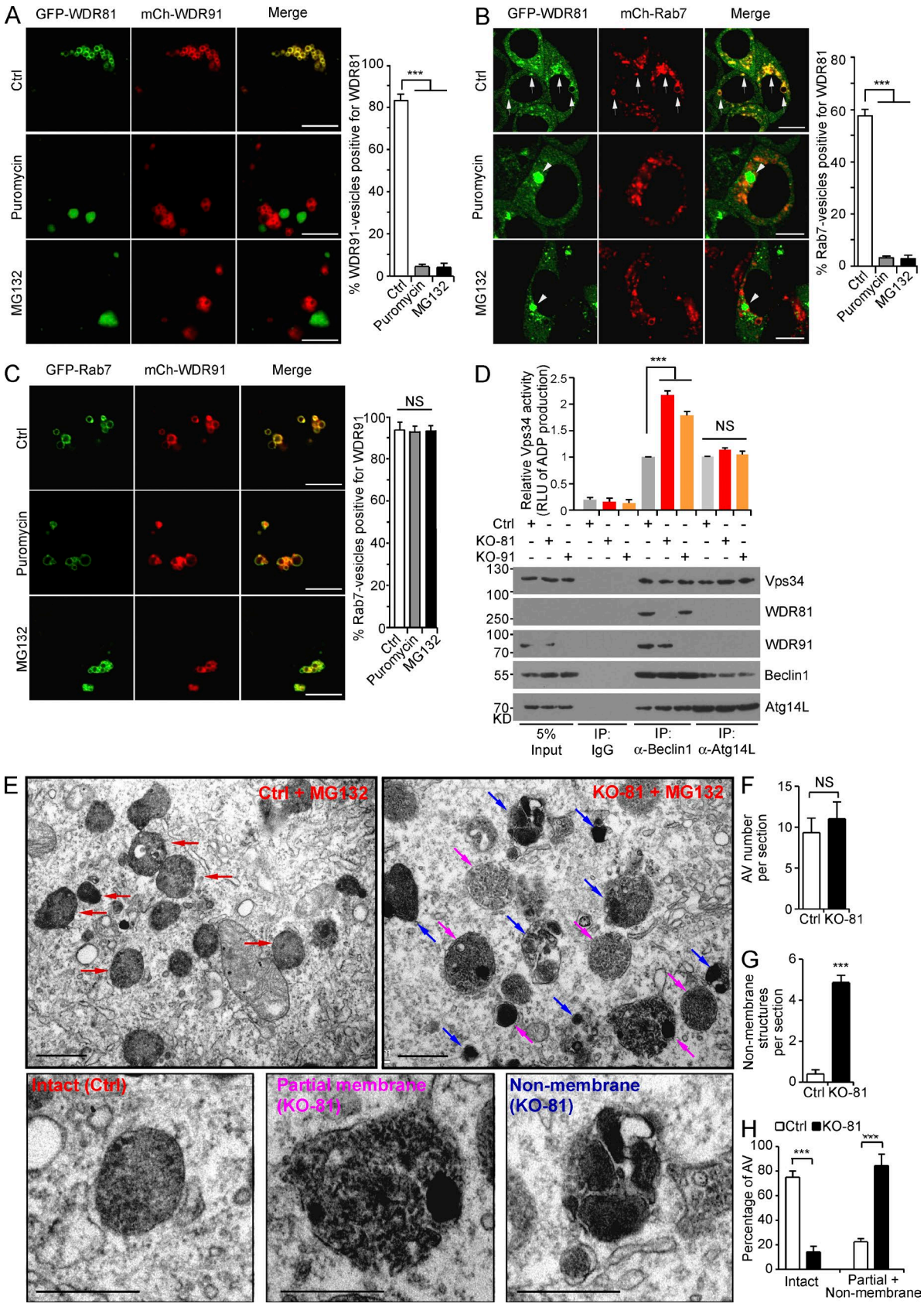

Figure 3. **WDR81 acts in aggrephagy independently of the endosomal WDR81-WDR91 complex.** (A) Colocalization of GFP-WDR81 with mCh-WDR91 in HeLa cells treated with or without puromycin or MG132 (left). Quantification of WDR91-vesicles positive for WDR81 (right). (B) Colocalization of GFP-WDR81 with mCh-Rab7 in HeLa cells treated with or without puromycin or MG132 (left). Arrows indicate WDR81-positive Rab7 vesicles; arrowheads indicate WDR81 foci that do not localize to Rab7 vesicles. Quantification of Rab7-vesicles positive for WDR81 (right). (C) Colocalization of GFP-Rab7

with truncated WDR81 proteins fused with GFP, we found that p62 foci efficiently recruited WDR81 truncations containing the N-terminal 1–650 aa (WDR81(1–650)), which include the BEACH domain. Other WDR81 truncations lacking this region failed to colocalize with p62 (Fig. 4 D). Using immunoprecipitation (IP), we found that HA-p62 physically interacted with Flag-tagged full-length WDR81 and WDR81(1–650), but not the WD40-repeat region (aa 1,637–1,940, WDR81(WD40); Fig. 4, E–G). In vitro, GST-fused p62, but not GST, efficiently pulled down either full-length WDR81 or WDR81(1–650), but not WDR81(WD40) (Fig. 4 H). GST-p62 also pulled down ^{35}S-labeled full-length WDR81 (Fig. 4 I). Altogether, these findings suggest that WDR81 and p62 directly interact with one another and that the BEACH-containing N terminus (1–650) of WDR81 is sufficient and necessary for this interaction.

We then investigated which domain in p62 is required for the interaction with WDR81 by coexpressing GFP-WDR81(1–650) with a series of mCh-p62 truncations. We found that p62 fragments containing the PB1 domain (aa 1–120), including aa 1–120, 1–180, and 1–385, formed foci to which GFP-WDR81(1–650) was recruited (Fig. 4 J). Longer fragments had a stronger effect on WDR81(1–650) recruitment. In contrast, p62 truncations without the PB1 domain did not show obvious colocalization with WDR81 (Fig. 4 J). Using in vitro pull-down assays, we found that GST-p62 and GST-p62(PB1) directly interacted with ^{35}S-labeled WDR81(1–650) (Fig. 4 K). Moreover, the p62 truncations aa 1–120, 1–180, and 1–385, but not 121–320 or 321–440, interacted with WDR81(1–650) in co-IP assays (Fig. 4 L). These data demonstrated that the PB1 domain mediates the interaction of p62 with WDR81.

WDR81 promotes the interaction of p62 with Ub proteins

To understand how the interaction of WDR81 may affect p62 function, we investigated the binding of p62 with Ub proteins in KO-81 cells. To this end, we immunoprecipitated p62 and examined the coprecipitated Ub proteins. Whereas the levels of total Ub proteins and K63-Ub proteins were strongly enhanced in KO-81 cells, the amount of total Ub proteins or K63-Ub proteins coprecipitated with p62 was much lower in KO-81 cells than in control cells (Fig. 5, A and B). K48-Ub proteins were unaffected (Fig. 5 C). Consistent with this, the proportion of Ub protein foci positive for p62 in KO-81 cells, regardless of proteotoxic stress (e.g., MG132 treatment), was significantly decreased compared with that in control HeLa cells treated with MG132 (Fig. 5 D). In contrast, p62-associated total Ub and K63-Ub proteins, but not K48-Ub proteins, were greatly increased in HEK293 cells overexpressing Flag-WDR81 (Fig. 5, E–G). These data suggest that WDR81 facilitates the interaction of p62 with K63-Ub proteins. To corroborate this point, we coexpressed Flag-WDR81 and HA-p62 with Myc-Ub(K63) or Myc-Ub(K48) in HEK293 cells and immunoprecipitated HA-p62. Co-expression of Flag-WDR81 strongly increased the association with HA-p62 of Myc-Ub(K63)-labeled, but not Myc-Ub(K48)-labeled, proteins (Fig. 5, H and I). KO-81 HeLa cells or HEK293 cells expressing Flag-WDR81 did not show an obvious change in p62 phosphorylation at Ser 403, though this phosphorylation was increased by BFA1 treatment as reported previously (Fig. 5 J; Matsumoto et al., 2011; Lim et al., 2015). Thus, WDR81 did not facilitate p62 interaction with K63-Ub proteins by changing p62 phosphorylation.

We also examined whether WDR81 associates with Ub proteins in the absence of p62. For this purpose, we expressed Flag-WDR81 in wild-type or *p62*$^{-/-}$ immortalized baby mouse kidney epithelial cells (Guo et al., 2011a) and then performed IPs. We found that Ub proteins were coimmunoprecipitated with Flag-WDR81 in wild-type cells (Fig. 5 K). The association of Ub proteins with WDR81 is probably noncovalent, because very low levels of Ub proteins were coprecipitated with WDR81 when IPs were performed with SDS-containing RIPA buffer (+RIPA), which is known to prevent noncovalent interactions (Seibenhener et al., 2004). In *p62*$^{-/-}$ cells, the amount of Ub proteins coprecipitated with Flag-WDR81 was also markedly reduced, suggesting that p62 is important for the association of WDR81 with Ub proteins (Fig. 5 K). Collectively, these findings suggest that WDR81 cooperates with p62 to promote recognition of Ub proteins for degradation through autophagy.

WDR81 is critical for LC3C recruitment by Ub proteins

Given that WDR81 promotes cargo recognition by interacting with p62 during aggrephagy, we further asked if WDR81 plays a role in facilitating the recruitment of major autophagy factors to Ub protein aggregates. The recruitment of ULK1, ATG12, Vps34, or ATG14L by Ub protein foci was similar in MG132-treated control HeLa cells and in KO-81 cells with or without MG132 treatment (Fig. S5 A). However, the proportion of Ub protein foci that were positive for LC3 family proteins in KO-81 cells was significantly reduced compared with that in control cells treated with MG132 (Fig. 6 A), suggesting that WDR81 is important for recruitment of LC3 family members by Ub proteins. To test this hypothesis, we investigated whether WDR81 interacts with individual members of the LC3 or GAB ARAP subfamilies. Whereas no obvious coprecipitation of mCh-LC3B or mCh-LC3A with Flag-WDR81 was detected, mCh-LC3C clearly coimmunoprecipitated with Flag-WDR81 (Fig. 6, B and C). In addition, mCh-tagged GABARAP and GABARAPL1, but not GABARAPL2, showed very weak association with Flag-WDR81 (Fig. 6 C). These results indicate that WDR81 preferentially interacts with LC3C. Consistent

with mCh-WDR91 in HeLa cells treated without or with puromycin or MG132 (left). Quantification of Rab7-vesicles positive for WDR91 (right). (D) Loss of WDR81 or WDR91 does not affect the activity of the Atg14–Beclin1–Vps34 complex. Beclin1 or Atg14L was immunoprecipitated from control (ctrl), KO-81, and KO-91 HeLa cells. Precipitated proteins were detected with antibodies for the indicated proteins (bottom). Equal amounts of precipitated proteins from each genotype were examined for Vps34 activity by measuring the luminescence (relative light units [RLU]) of ADP converted from ATP. Data (mean ± SEM) were from three independent experiments and are normalized to Vps34 activity in Ctrl cells (top). (E) Representative TEM images of control and KO-81 HeLa cells with MG132 treatment. Red arrows indicate cargo-containing autophagic vesicles (AVs) with intact membranes in control HeLa cells. Pink arrows indicate proteinaceous structures with partial membranes in KO-81 cells. Blue arrows indicate non–membrane-enclosed proteinaceous structures in KO-81 cells. Representative structures indicated by red, pink, and blue arrows are magnified at the bottom. (F–H) Quantification of AV numbers (F), non–membrane-enclosed proteinaceous structures (G), and intact or defective AVs observed by TEM (H). The treatment of cells with puromycin or MG132 was performed as in Fig. 1. For all quantifications, data (mean ± SEM) were from three independent experiments and analyzed using ANOVA. ***, $P < 0.001$; NS, not significant. Bars: (fluorescence images) 10 µm; (TEM images) 5 µm.

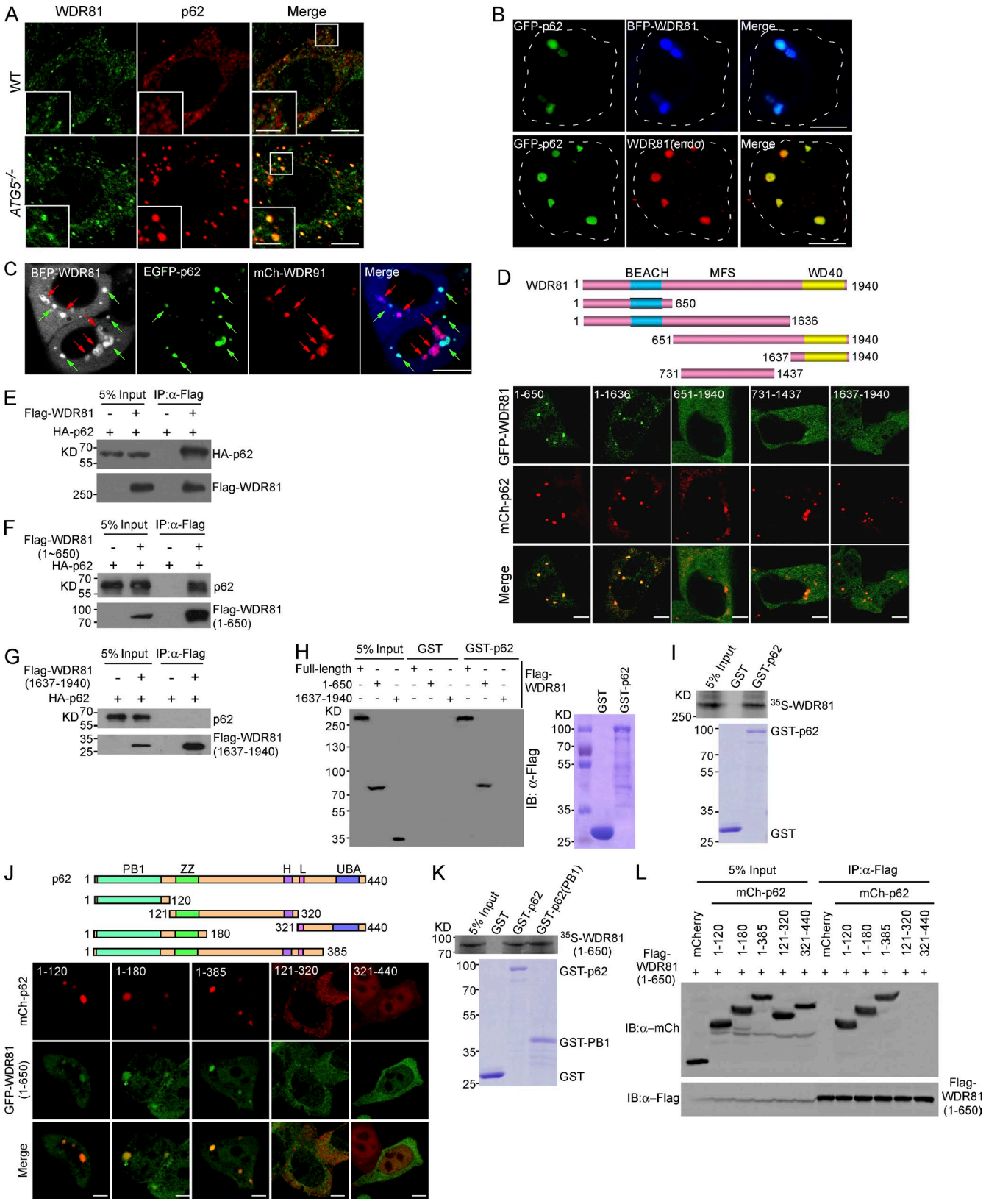

Figure 4. **WDR81 interacts with p62.** (A) Immunostaining of p62 and WDR81 in wild-type (WT) and *ATG5*$^{-/-}$ MEF cells. Insets show a magnified view (1.8×) of the boxed area in the merged images. (B) Images of BFP-WDR81 and GFP-p62 coexpressed in HeLa cells (top row); and images of overexpressed GFP-p62 and immunostained endogenous WDR81 (bottom). Dashed lines indicate the cell outline. (C) Colocalization of BFP-WDR81 with GFP-p62 (green arrows) or mCh-WDR91 (red arrows) in HeLa cells. (D) Colocalization of GFP-tagged WDR81 truncations with mCherry-p62 (mCh-p62) in HeLa cells. Schematic representations of the WDR81 truncations are shown in the top panel; the colocalizations are shown in the bottom panel. (E–G) Co-IP of HA-p62 with Flag-WDR81 (E), of HA-p62 with Flag-WDR81(1–650) (F), and of HA-p62 with Flag-WDR81(WD40) (G) in HEK293 cells. IPs were performed

with this notion, coexpressed BFP-WDR81 and GFP-LC3C colocalized to Myc-Ub foci, and this colocalization became more obvious after exposure to MG132 (Fig. S5 B). In KO-81 cells, however, a significant proportion of Myc-Ub foci were negative for GFP-LC3C, whereas the colocalization of GFP-LC3B with Ub protein foci was unchanged regardless of MG132 treatment (Fig. 6, D–F). Collectively, these findings suggest that WDR81 preferentially interacts with LC3C and promotes its recruitment by Ub proteins.

Using quantitative RT-PCR or a human LC3C–specific antibody, we found that LC3C is expressed in both control and KO-81 HeLa cells, as well as in HEK293 and SH-SY5Y cells (Fig. S5, C–E). Intriguingly, no information about the LC3C gene was found in the mouse genome database. Nevertheless, an LC3C-like protein comparable to human LC3C was detected in both wild-type and *ATG5*$^{-/-}$ MEF cells with the same LC3C-specific antibody, and *ATG5*$^{-/-}$ MEF cells seemed to have a higher level of this LC3C-like protein (Fig. S5 F). In addition, whereas siLC3A and siLC3B specifically knocked down LC3A and LC3B in *ATG5*$^{-/-}$ MEF cells, respectively, the level of the LC3C-like protein was not changed by these siRNA treatments (Fig. S5 G). Like *ATG5*$^{-/-}$ MEF cells, the brain of WDR81 conditional knockout (cKO) mice (see below) also has a higher level of the LC3C-like protein than the wild type (Fig. S5 H). These findings suggest that mice probably have an LC3C-like protein that might act similarly to human LC3C in selective autophagy. In HeLa cells, siRNA of LC3C, which did not affect other LC3 isoforms (Fig. 6, G and H), led to formation of Ub protein focal structures that costained with endogenous p62 or WDR81 and were immunostained much more intensely than the small puncta in control cells (Fig. 6, I and J). Immunoblotting analysis confirmed that the levels of Ub proteins and p62 were indeed greatly elevated after siLC3C treatment (Fig. 6 K). Similarly, siLC3C strongly increased the protein level of stably expressed Flag-WDR81 (Fig. 6 L). Thus, LC3C is essential for clearance of Ub proteins, p62, and WDR81, suggesting that LC3C plays a critical role in aggrephagy.

WDR81 interacts with LC3C through LIRs

We next investigated which domain in WDR81 is responsible for interaction with LC3C. Using co-IPs, we found that GFP-tagged WDR81(1–650), but not other regions, coprecipitated with mCh-LC3C (Fig. 7 A). Further co-IP analysis revealed that the BEACH domain (WDR81(341–650)) was sufficient and necessary for WDR81 to interact with LC3C (Fig. 7 B). Based on these results, we sought to identify amino acid residues in this region that are required for interaction with LC3C. Interestingly, this region contains two putative canonical LIRs, which are found in several autophagy receptors such as p62, NBR1, and FUNDC1 (Pankiv et al., 2007; Kirkin et al., 2009a; Liu et al., 2012). These putative LIRs are also found in WDR81 homologues in multiple species (Fig. S5 I). In addition, two candidate noncanonical LIRs (CLIRs), which are similar to that in NDP52, are also found in this region (von Muhlinen et al., 2012; Fig. 7 C). We thus mutated key residues in these putative LIRs or CLIRs and examined the interaction with LC3C. As shown in Fig. 7 D, mutations in LIR1 (W544A/L547A, LIR1^{AA}) and LIR2 (S577A/Y578A/V581A, LIR2^{AA}), but not the putative CLIRs, abrogated the interaction of WDR81(341–650) with mCh-LC3C in co-IP assays. Similarly, whereas full-length Flag-WDR81 clearly coimmunoprecipitated with mCh-LC3C, Flag-WDR81 containing LIR1^{AA}, LIR2^{AA}, or both, failed to associate with mCh-LC3C in co-IP assays (Fig. 7 E). Using GST pull-down assays, we confirmed that GST-LC3C, but not GST, pulled down full-length Flag-WDR81 but not Flag-WDR81 containing LIR mutations (Fig. 7 F). Altogether these findings suggest that WDR81 interacts with LC3C through canonical LIRs.

To determine the requirement for the WDR81-LC3C interaction in degradation of p62, we examined whether wild-type or mutant WDR81 rescued the elevation of p62 in KO-81 cells. Expression of Flag-WDR81 reduced the accumulation of p62 foci and the elevation of p62 in KO-81 cells to a level comparable to that in control HeLa cells (Fig. 7, G and H). However, overexpression of Flag-WDR81 carrying LIR1^{AA}, LIR2^{AA}, or both did not obviously rescue the accumulation of p62 in KO-81 cells (Fig. 7, G and H). These results suggest that the interaction of WDR81 with LC3C is required for p62 degradation.

Interaction of LC3C with WDR81 is essential for aggrephagy

We next investigated the requirement for LC3C to interact with WDR81 in aggrephagy. Given that LC3 family members normally interact with LIR-containing proteins through a hydrophobic pocket containing a "W-site" and an "L-site" (Noda et al., 2010) and that WDR81 interacts with LC3C, but not LC3B, we mutated the critical W-site and L-site residues in LC3C to those in LC3B and tested the interaction with WDR81 (von Muhlinen et al., 2012). Our co-IP results showed that neither the K32Q/F33H mutations, which affect the W-site, nor the L64V/F69L mutations, which affect the L-site, had an obvious effect on the interaction of mCh-LC3 with Flag-WDR81 (Fig. 7 I). However, the K32Q/F33H/L64V/F69L mutations, which changed both sites in LC3C to those of LC3B, greatly reduced the interaction of LC3C with WDR81 (Fig. 7 I). In contrast, the same mutations strongly increased the interaction of LC3C with p62 compared with wild-type LC3C (Fig. S5 J). These results suggest that LC3C interacts with WDR81 through the W-site and L-site. Furthermore, overexpression of the K32Q/F33H/L64V/F69L LC3C mutant failed to rescue the accumulation of p62 induced by siRNA of LC3C, in sharp contrast to the full rescuing effect of wild-type LC3C (Fig. 7 J). Collectively, these results suggest that the interaction with WDR81 is important for the functional role of LC3C in aggrephagy.

using Flag antibody, and precipitated proteins were detected with the indicated antibodies. (H) Interaction of GST-p62 with Flag-WDR81. Purified GST and GST-p62 (left) immobilized on glutathione-Sepharose beads were incubated for 12–16 h at 4°C with lysates of HEK293 cells expressing Flag-WDR81, Flag-WDR81(1–650), or Flag-WDR81(WD40). After extensive washing, bound proteins were subjected to immunoblotting (IB) with antibodies to Flag (right). (I) In vitro interaction of GST-p62 with ^{35}S-labeled WDR81. (J) Colocalization of GFP-WDR81(1–650) with mCh-tagged p62 truncations in HeLa cells. Schematic representations of the p62 truncations are shown in the top panel and protein colocalizations are shown in the bottom panel. Bars, 10 µm. H, leucine-rich nuclear export signal; L, LC3-interaction region; PB1, Phox and Bem1p domain; UBA, ubiquitin-associated domain; ZZ, ZZ-type zinc-finger domain. (K) In vitro interaction of GST-p62, GST-p62(PB1) with ^{35}S-labeled WDR81(1–650). (L) Co-IP of mCh-tagged p62 truncations with Flag-WDR81(1–650) in HEK293 cells. IPs were performed using Flag antibody, and precipitated proteins were detected with antibodies to Flag and mCherry. Bars: (main images) 10 µm; (A, insets) 5 µm.

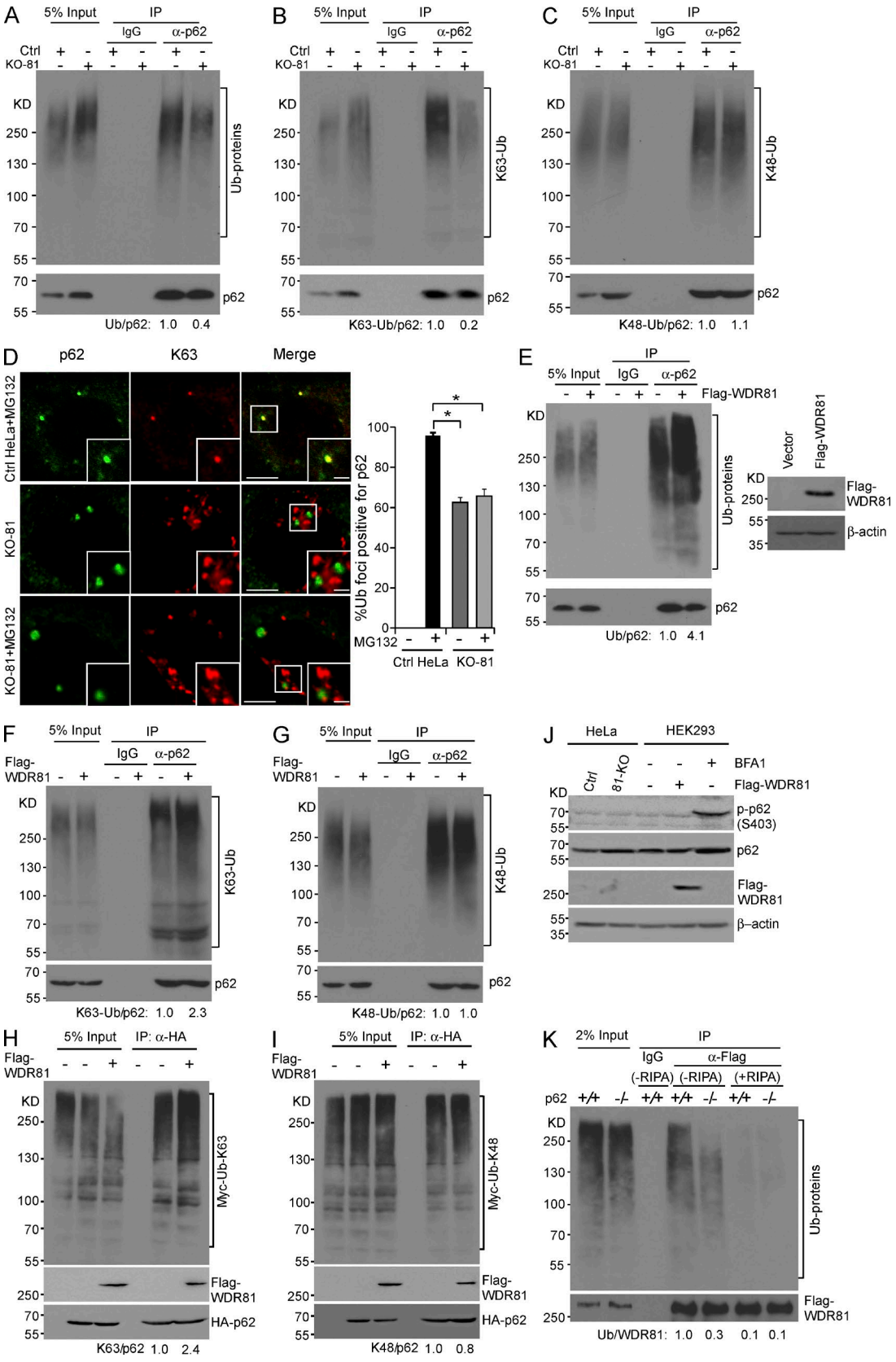

Figure 5. **WDR81 promotes the binding of p62 with Ub proteins.** (A–C) IP of endogenous p62 in Ctrl or KO-81 cells with anti-p62 antibodies. Coprecipitated Ub proteins were detected with antibodies to Ub (A), K63-Ub (B), and K48-Ub (C). The ratios of Ub proteins/p62 in the precipitates are indicated at the bottom. (D) Immunostaining of p62 and K63-Ub in Ctrl or KO-81 cells treated without or with 10 µM MG132 (12 h). Insets show magnified (1.8×) views of the box in the merged images. Bars: (main images) 10 µm; (insets) 5 µm. Quantification of p62-positive Ub foci is shown in the right panel. Data (mean ± SEM) were derived from three independent experiments and analyzed using ANOVA. *, $P < 0.05$. (E–G) IP of endogenous p62 in HEK293 cells

WDR81 deficiency leads to accumulation of p62 bodies in mouse brain

In mice, *WDR81* expression was detected in several tissues and was highest in the brain (Fig. 8 A). This is consistent with a previous study on human WDR81 (Gulsuner et al., 2011). To investigate whether WDR81 promotes aggrephagy in mouse brain as in human cells, we generated mice (*WDR81^{fff}*) with loxP sites flanking exons 2–4 of the *WDR81* gene, and then crossed them with mice expressing the Cre recombinase driven by the promoter of the brain-abundant *Nestin* gene (*Nestin-Cre*). This led to deletion of exons 2–4, resulting in a frameshift and a premature stop codon in exon 5 of the *WDR81* gene in the brain of *WDR81^{fff}:Nestin-Cre* mice (hereafter referred to as *WDR81^{fff}* cKO mice; Fig. 8 B).

WDR81^{fff} cKO mice were born at the expected Mendelian frequency, but most of them died quickly within a few hours after birth (Fig. 8 C), apart from a few escapers that grew into adults. The death of *WDR81^{fff}* cKO mice might result from the unexpectedly high recombination efficiency of Cre controlled by the *Nestin* promoter (Haigh et al., 2003). To investigate the effect of WDR81 inactivation on protein aggregates in the brain, we examined brain sections and performed immunostaining of p62 and ubiquitin. Intriguingly, no obvious brain abnormalities were observed in *WDR81^{fff}* cKO mice, unlike the defective development of the corpus callosum, third ventricle, fourth ventricle, and cerebellum in human CAMRQ2 patients carrying a WDR81 mutation (Gulsuner et al., 2011). However, p62 foci strongly accumulated in the cortex of both dead and surviving *WDR81^{fff}* cKO mice at postnatal day 0 (P0), and the dead mice had higher levels of accumulation of p62 foci (Fig. 8 D). Both Ub-positive and Ub-negative p62 foci were observed (Fig. 8 E). Accumulation of p62 bodies was also observed in the developing cortex at embryonic day 14.5 (E14.5) and E18.5 (Fig. 8, F and G). In surviving adult *WDR81^{fff}* cKO mice at P180, p62 foci were found not only in the cortex but also in the striatum, whereas the brain did not show any obvious abnormalities (Fig. 8 H).

To determine the cell types in which WDR81 functions, we performed immunohistochemistry analysis and found that WDR81 is mainly expressed in neurons, but not astrocytes, in the brain (Fig. 9, A–C). Consistent with this, we found that p62 foci were mainly present in NeuN-positive neurons, but not GFAP-positive astrocytes (Fig. 9, D and E). These data suggest that WDR81 is required for preventing protein aggregate accumulation in neurons. To consolidate this conclusion, we induced *WDR81* inactivation in the striatum of adult *WDR81^{fff}* mice by stereotaxically grafting lentivirus expressing a GFP-fused Cre (Cre-GFP) or a GFP-fused Cre truncation (ΔCre-GFP) that has no recombinase activity (Fig. 9 F). Grafting of lentivirus expressing Cre-GFP effectively ablated *WDR81* expression (Fig. 9 F). Consistent with this, accumulation of p62 foci was detected over time in the NeuN-positive neurons, but not GFAP-positive astrocytes, in the brain regions infected by viruses expressing Cre-GFP, whereas no p62 foci were observed in the contralateral regions infected with ΔCre-GFP-expressing viruses (Fig. 9, G and H). Collectively, these findings provide further evidence that WDR81 plays an important role in removing aggregated proteins in neuronal cells in mice. Of note, these results do not exclude the possibility that WDR81 participates in other selective autophagy processes in mice, as the accumulated p62 or Ub foci in WDR81 cKO mouse brain may include other selective autophagy cargoes.

Discussion

In this study, we identify WDR81 as an essential factor in autophagy-dependent clearance of Ub proteins. Loss of WDR81 function leads to accumulation of Ub proteins and the autophagy receptor p62 in cells and mouse brains. WDR81 associates with ubiquitinated and aggregated proteins, where it acts in complex with p62. WDR81 inactivation significantly reduced, whereas its overexpression strongly enhanced, the association of p62 with Ub proteins. This suggests that the interaction of WDR81 with p62 promotes cargo recognition for aggrephagy. In addition, loss of WDR81 specifically reduced the recruitment of LC3C to ubiquitinated proteins. Our data further indicate that WDR81 interacts with LC3C, but not other LC3 subfamily members. The canonical LIRs in WDR81 mediate the interaction with LC3C through the LC3C-specific hydrophobic pocket. These findings collectively suggest that WDR81 coordinates p62-dependent recognition of Ub proteins with LC3C-mediated assembly of autophagosomes, thereby facilitating Ub protein clearance through autophagy.

Although WDR81 was found to act in complex with WDR91 to regulate endosome maturation (Liu et al., 2016), the findings in this study suggest that neither WDR81 nor WDR91 affects the activity of the autophagic PI3K complex. The function of WDR81 in aggrephagy does not require WDR91. This is supported by the fact that WDR81, but not WDR91, is recruited by Ub protein foci and p62 bodies and that KO-91 cells do not accumulate enlarged foci of Ub proteins and p62. In addition, WDR81 separately interacts with p62 and WDR91. Thus, WDR81 plays dual functions in aggrephagy and endosome maturation by forming complexes with p62/LC3C or WDR91, respectively.

Previously it has been shown that LC3C interacts with NDP52 to mediate antibacterial autophagy. This interaction, conferred by a noncanonical LIR in NDP52, executes selective autophagic removal of bacteria (von Muhlinen et al., 2012). Our findings about the WDR81–LC3C interaction establish the essential role of LC3C in aggrephagy. We found that LC3C interacts through its hydrophobic pocket with the canonical LIRs of WDR81. Interestingly, the hydrophobic pocket residues in LC3C are more closely related to those in GABARAP subfamily members. For example, K32, L64, and

with or without Flag-WDR81 overexpression. Coprecipitated Ub proteins were detected with antibodies to ubiquitin (E), K63-Ub (F), and K48-Ub (G). The ratios of Ub proteins/p62 in the precipitates are indicated at the bottom. Expression of Flag-WDR81 is shown in the right in E. (H and I) IP of HA-p62 with Myc-Ub(K63) (H) or Myc-Ub(48) (I) proteins with or without coexpression of Flag-WDR81 in HEK293 cells. Coprecipitated Ub proteins and WDR81 were detected with antibodies to Myc or Flag. The ratios of Ub proteins/p62 in the precipitates are indicated at the bottom. (J) Phosphorylation of p62 at Ser 403 in control and KO-81 HeLa cells, and in HEK293 cells with Flag-WDR81 overexpression or BFA1 treatment. Western blot was performed with the indicated antibodies. (K) Flag-WDR81 was expressed in wild-type (*p62$^{+/+}$*) or *p62$^{-/-}$* cells and immunoprecipitated in regular IP buffer or RIPA buffer. Precipitated proteins were detected with antibodies to Flag and Ub. Fold changes of Ub/WDR81 in the precipitates were normalized to control and are indicated at the bottom.

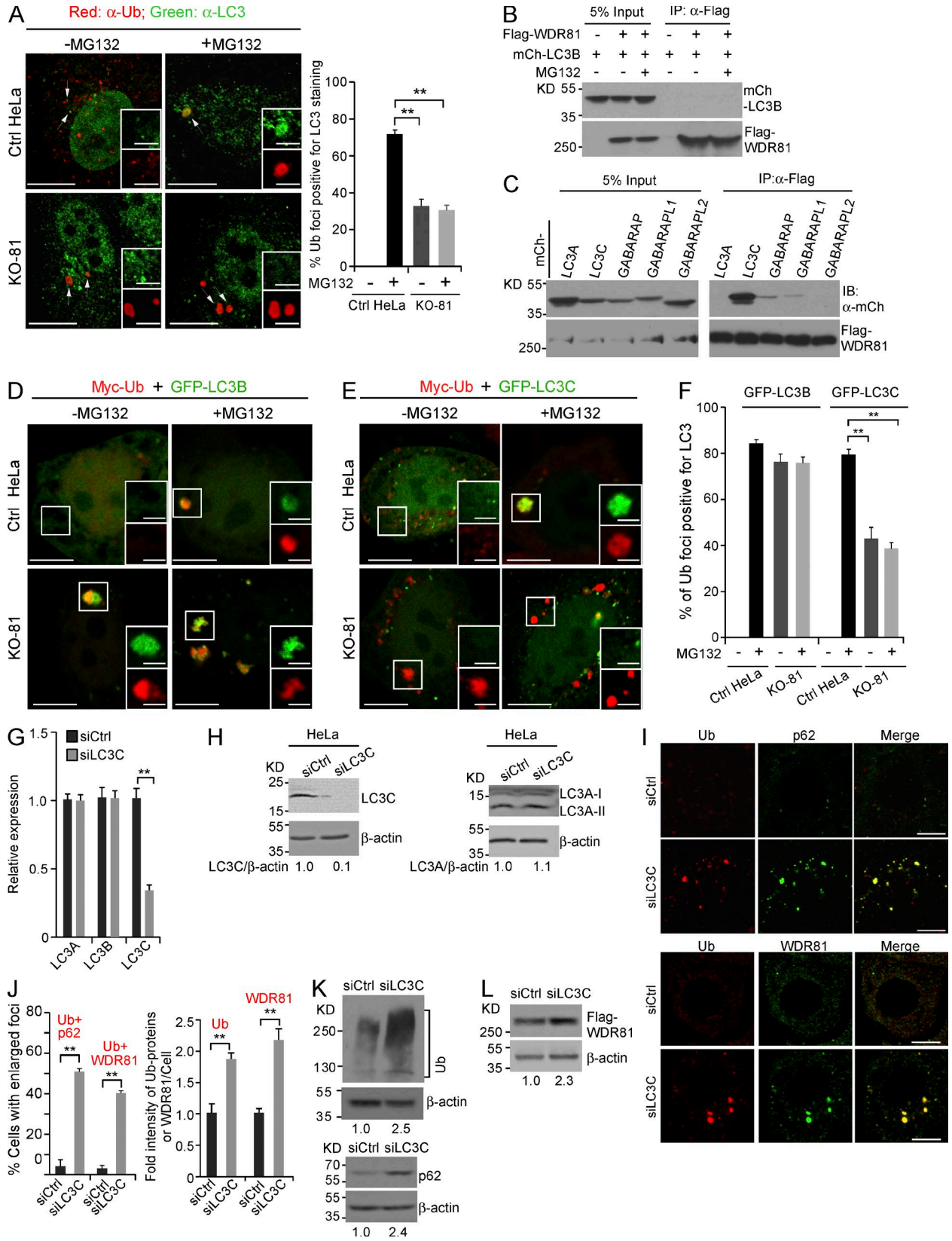

Figure 6. **WDR81 promotes LC3C recruitment to Ub proteins.** (A) Immunostaining of LC3 and Ub in Ctrl or KO-81 HeLa cells treated without or with 10 µM MG132 (12 h; left). The LC3 antibody reacts with LC3A, B, and C. Insets show images of LC3 foci (green) and Ub proteins (red) indicated by arrows in the main panels. Bars: (main images) 10 µm; (insets) 5 µm. Quantification of LC3-positive Ub foci (right). Data (mean ± SEM) were derived from three independent experiments. Comparisons were made using ANOVA. **, $P < 0.01$. (B) Co-IP of Flag-WDR81 with LC3B in HEK293 cells without or with 10 µM MG132 treatment (12 h). IPs were performed with Flag antibody, and precipitated proteins were detected with antibodies to mCherry and Flag. (C) Co-IP of Flag-WDR81 with individual members of the LC3 or GABARAP subfamilies in HEK293 cells. IPs were performed with Flag antibody, and precipitated

F69 in LC3C are conserved in GABARAP members, but not in LC3A or LC3B (von Muhlinen et al., 2012). Nevertheless, WDR81 strongly interacts with LC3C but weakly with GABARAPs, whereas no interaction with LC3A and LC3B was observed. Thus, other residues in the hydrophobic pocket in LC3C may also contribute to the preferential interaction with WDR81. In addition, because loss of WDR81 does not completely abrogate LC3C recruitment to Ub proteins, other LC3C-interacting adaptor proteins, for example ALFY or NDP52, likely act redundantly with WDR81 in aggrephagy. Our results, together with those reported previously, suggest that the specific role of LC3C in selective autophagy is achieved by interacting with different adaptors/receptors.

Our findings suggest that the BDCP (BEACH domain–containing protein) family members WDR81 and ALFY play distinct roles in aggrephagy (Cullinane et al., 2013). Both WDR81 and ALFY facilitate aggrephagy by interacting with p62. Nevertheless, ALFY appears to act as a scaffold during the interaction of the autophagy factors Atg5-12 with the phagophore membrane without being degraded (Clausen et al., 2010; Filimonenko et al., 2010). In contrast, WDR81 does not obviously affect assembly of core autophagy factors but is degraded together with autophagy cargos and the p62 receptor. In addition, a recent study revealed that ALFY directly interacts with GABARAPs, but it interacts with LC3C much more weakly (Lystad et al., 2014). In our study, we found that WDR81 strongly interacts with LC3C but weakly with GABARAPs. Thus, the preferential interactions of WDR81 or ALFY with LC3C or GABARAPs likely play different roles in formation of autophagosomes during aggrephagy. Consistent with this notion, it has been shown that LGG-1 and LGG-2, the ATG8 homologues in *C. elegans*, bind to different substrates or ATG protein complexes in autophagic degradation of protein aggregates during *C. elegans* development (Wu et al., 2015).

A human *WDR81* mutation was found to be associated with CAMRQ2 syndrome, which manifests as quadrupedal locomotion, mental retardation, and cerebrocerebellar hypoplasia (Gulsuner et al., 2011). In this study, we revealed a distinct role of WDR81 in removing ubiquitinated and aggregated proteins. This is strongly supported by the fact that WDR81 knockout leads to a strong accumulation of p62 bodies in the cortex and striatum in mouse brains. WDR81 may also participate in clearance of damaged mitochondria, because mice carrying a WDR81 point mutation accumulate aberrant mitochondria in Purkinje cell dendrites (Traka et al., 2013). Although no LC3C gene information was found in the mouse genome database, an LC3C-like protein, which seems to be degraded in a WDR81- and ATG5-dependent manner (Fig. S5, F and H), might be involved in aggrephagy or other selective autophagy processes. It is possible that WDR81 acts together with this LC3C-like protein in mice, similar to the WDR81–LC3C interaction in human cells. Future studies will determine the identity of the LC3C-like protein and how it functions. In addition, although WDR81 cKO mice did not phenocopy the defective brain development in CAMRQ2 patients, the accumulation of aggregated proteins or damaged mitochondria may impair the function of neurons and render them sensitive to induction of cell death, a process that is implicated in neurodegenerative disease (Filimonenko et al., 2007; Moscat and Diaz-Meco, 2009; Menzies et al., 2015). Moreover, we and others recently showed that WDR81 is important for early-to-late endosome conversion, a key step in intracellular trafficking (Liu et al., 2016; Rapiteanu et al., 2016). Given the multifunctional properties of WDR81, CAMRQ2 syndrome may result from diverse defective cellular processes that lead to developmental defects. Importantly, mutations in several other BDCP family members are found to be associated with diseases, including Chediak–Higashi syndrome, immune deficiency, autism, gray platelet syndrome, and systemic lupus erythematous (Cullinane et al., 2013). It will therefore be of great interest to explore whether these BDCP proteins act similarly to WDR81 or ALFY in regulating intracellular trafficking or autophagy-related cellular processes.

Materials and methods

Cell culture, reagents, and transfection

Cells were cultured at 37°C with 5% CO_2 in DMEM supplemented with 10% FBS (HyClone), 100 U/ml penicillin, and 100 mg/ml streptomycin. *ATG5*$^{-/-}$ MEF cells were provided by N. Mizushima (University of Tokyo, Tokyo, Japan). *p62*$^{-/-}$ immortalized baby mouse kidney cells were provided by E. White (Rutgers University, New Brunswick, NJ). Wild-type and *ATG12*$^{-/-}$ NRK cells were gifts from L. Yu (Tsinghua University, Beijing, China). Transfections were performed with Lipofectamine 2000 (Invitrogen) or Vigofect (Vigorous Biotechnology Beijing Co., Ltd) according to the manufacturers' instructions. BFA1, puromycin, MG132, blasticidin, and zeocin were obtained commercially.

Antibodies

WDR81 antibodies were generated in guinea pigs and rabbits by injecting purified recombinant GST-WDR81(332–604). WDR91 antibody was generated in mouse by injecting GST-WDR91(406–730). GFP and mCherry antibodies were generated in guinea pigs or rabbits by injecting recombinant proteins. Rabbit polyclonal antibodies to p62 (PM045), LC3 (PM036), and Beclin1 (PD017) and rat antibody to p-p62(S403) (D343-3) were purchased from Medical & Biological Laboratories. Rabbit polyclonal antibodies to human LC3A (ab62720) and LC3C (ab168813) were purchased from Abcam. Rabbit polyclonal antibodies to human LC3B (NB100-2220) were purchased from Novus

proteins were detected with antibodies to mCherry and Flag. (D–F) Colocalization of Myc-Ub with GFP-LC3B (D) or GFP-LC3C (E) in Ctrl and KO-81 cells treated without or with 10 µM MG132 (12 h). Insets show images of GFP-LC3B or GFP-LC3C foci (green) and Myc-Ub foci (red) in the boxes in the main panels. Bars: (main images) 10 µm; (insets) 5 µm. Quantification of Myc-Ub foci positive for GFP-LC3B or GFP-LC3C is shown in F. Data (mean ± SEM) were derived from three independent experiments. Comparisons were made using ANOVA. **, $P < 0.01$. (G) Quantitative RT-PCR analysis of the specificity and efficiency of siLC3C. The mRNA levels of LC3A, LC3B, and LC3C were normalized to siCtrl treatment; error bars represent SEM derived from three independent experiments. Comparisons were made using ANOVA. **, $P < 0.01$. (H) Western blot analysis of LC3C and LC3A in HeLa cells treated with siCtrl or siLC3C. (I) Colocalization of endogenous Ub proteins with p62 or WDR81 in HeLa cells treated with siCtrl or siLC3C. (J) Quantifications of enlarged Ub protein foci positive for p62 or WDR81 (left) and the intensity of Ub protein or WDR81 staining (right) in HeLa cells treated with siCtrl or siLC3C. ≥100 cells were analyzed for each treatment. Data representing mean ± SEM were derived from three independent experiments. Comparisons were made using ANOVA. **, $P < 0.01$. (K) Immunoblotting of U proteins (top) and p62 (bottom) in siCtrl- or siLC3C- treated HeLa cells. Fold changes in Ub proteins or p62 were determined by normalizing to the control and are indicated at the bottom. (L) Immunoblotting of Flag-WDR81 that was stably expressed in HeLa cells treated with siCtrl or siLC3C. The fold change in Flag-WDR81 was determined by normalizing to the control and is indicated at the bottom.

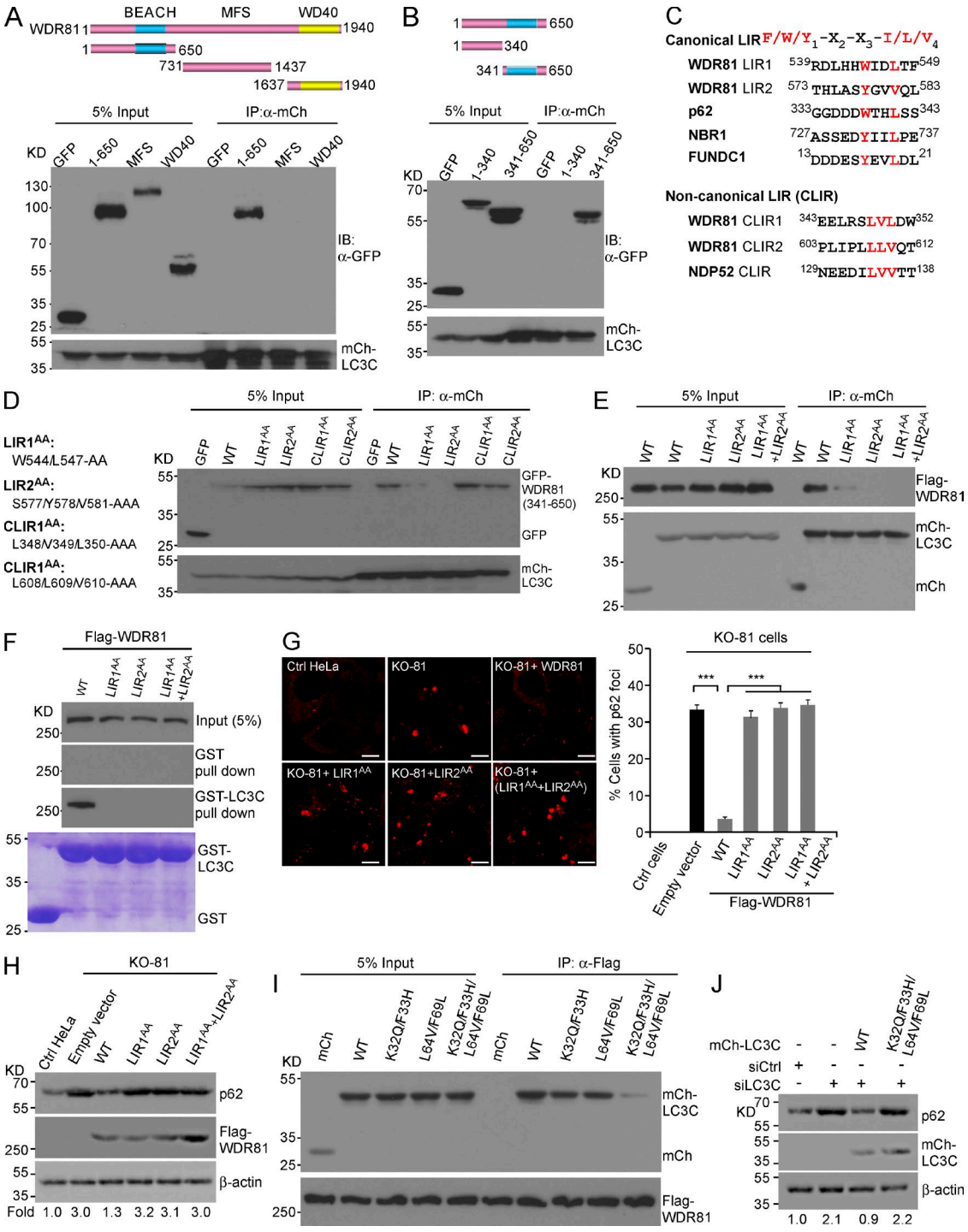

Figure 7. **WDR81 interacts with LC3C through two LIRs to facilitate aggrephagy.** (A and B) Co-IP of GFP-tagged WDR81 fragments with mCh-LC3C. Individual GFP-WDR81 fragments were coexpressed with mCh-LC3C in HEK293 cells. IPs were performed with mCherry antibody, and precipitated proteins were detected with antibodies to GFP and mCherry. (C) Alignment of canonical and noncanonical LIRs in WDR81 with those in p62, NBR1, FUNDC1, or NDP52. Conserved residues are shown in red. (D) Co-IP of mCh-LC3C with wild-type (WT), LIR, or CLIR mutants of GFP-WDR81(341–650) in HEK293 cells. WDR81 mutations are shown in the box. IPs were performed with mCherry antibody and precipitated proteins were detected with antibodies to GFP and mCherry. (E) Co-IP of mCh-LC3C with WT or the indicated LIR mutants of Flag-WDR81 full-length protein in HEK293 cells. IPs were performed as in A. (F) Pull-down of Flag-WDR81 by GST-LC3C. Purified recombinant GST and GST-LC3C immobilized on glutathione-Sepharose beads were incubated overnight at 4°C with lysates of HEK293 cells expressing Flag-WDR81 or the indicated Flag-WDR81 mutants. After extensive washing, bound proteins were subjected to Western blot with Flag antibody. (G and H) KO-81 HeLa cells were transfected with Flag-WDR81 or the indicated Flag-WDR81 mutants. 48 h later, cells were subjected to immunostaining (G) or immunoblotting (H) with p62 antibody. Quantification (mean ± SEM) of p62 in (G) is shown in the right panel. ***, $P < 0.001$. Bars, 10 µm. (I) Co-IP of Flag-WDR81 with WT or the indicated hydrophobic pocket mutants of LC3C in HEK293 cells. IPs were performed with Flag antibody, and precipitated proteins were detected with antibodies to Flag and mCherry. (J) Immunoblotting of p62 in siCtrl or siLC3C cells expressing RNAi-resistant LC3C (WT) or the LC3C (K32Q/F33H/L64V/F69) mutant in HEK293 cells. In H and J, fold changes in p62 levels were normalized to the control and are indicated at the bottom.

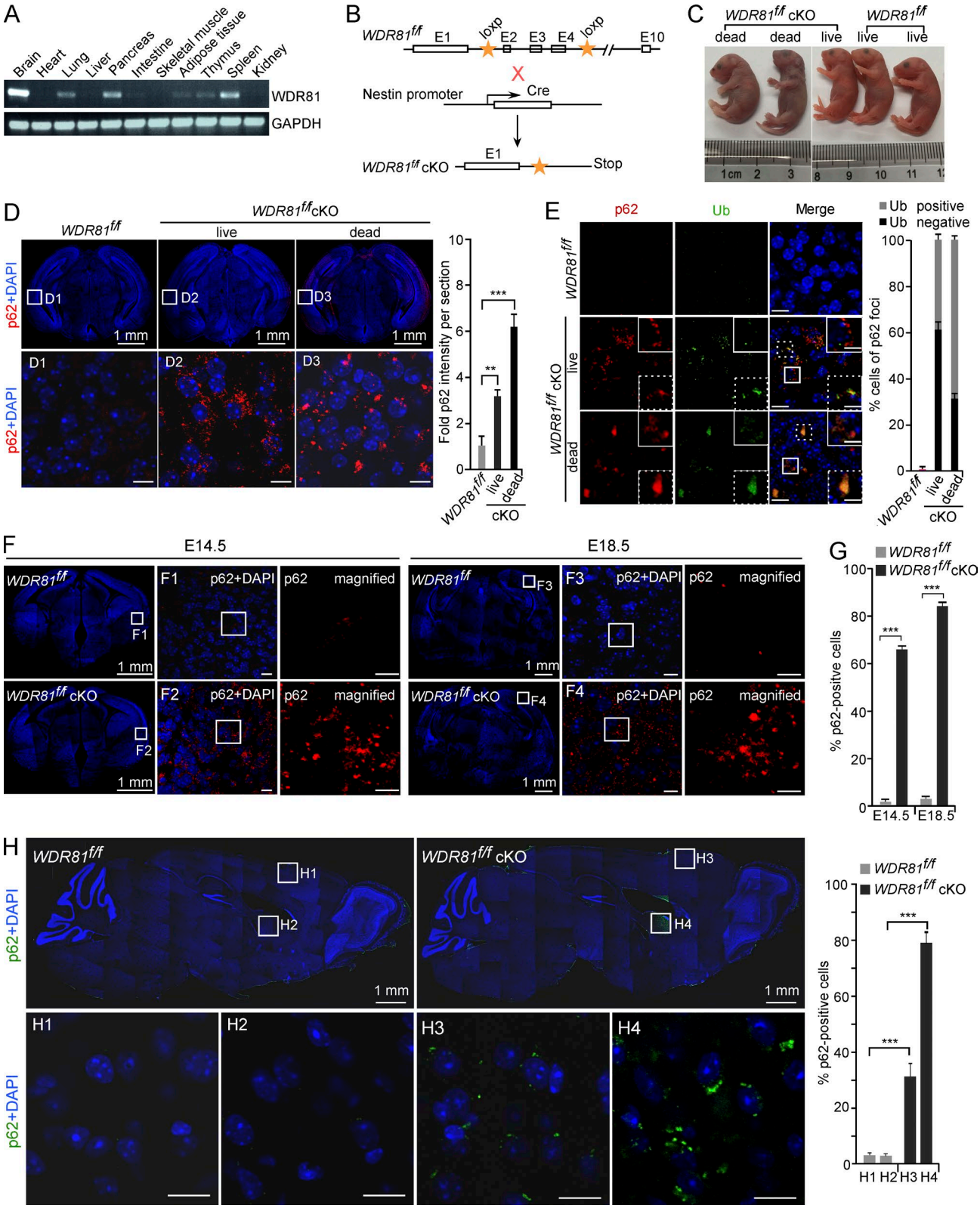

Figure 8. **WDR81 deficiency causes accumulation of p62-positive aggregates in mouse brain.** (A) RT-PCR analysis of *WDR81* expression in different mouse tissues. (B) Graphic representation of the scheme for generating *WDR81* conditional knockout (*WDR81*$^{f/f}$cKO) mice by crossing *WDR81*$^{f/f}$ mice with *Nestin-Cre* mice. (C) *WDR81*$^{f/f}$ cKO mice display perinatal lethality at P0. (D, left) Immunostaining of p62 in brain sections from *WDR81*$^{f/f}$ and *WDR81*$^{f/f}$ cKO mice at P0 (left). Nuclei are stained with DAPI. Boxed cortex regions in each image of whole brain sections (10x objective, top row) were observed under 60x objective and are shown in the bottom row (bars, 10 μm). (right) p62 intensities in the cortex were quantified and normalized to *WDR81*$^{f/f}$. 20 sections from four mice for each genotype were examined. Data (mean ± SEM) were analyzed using ANOVA. **, $P < 0.01$; ***, $P < 0.001$. (E) Immunostaining of p62 and Ub in brain sections from *WDR81*$^{f/f}$ and *WDR81*$^{f/f}$ cKO mice at P0 (left). Nuclei are stained with DAPI. Insets show magnified (2×) views of the dotted (Ub-positive) or solid (Ub-negative) box in the merged images. Bars: (main images) 10 μm; (insets) 5 μm. Quantification of p62 foci

Biologicals. Mouse monoclonal antibodies against Atg14L (M184-3), Atg12 (M154-3), and ubiquitin (MK-11-3) were purchased from Medical & Biological Laboratories. Monoclonal antibodies to ubiquitin (#3936) and Ub-K48 (#8081) were purchased from Cell Signaling Technology. Ub-K63 (14–6077-82) and Ub-K63 (Apu3) monoclonal antibodies were from eBioscience and EMD Millipore. Mouse monoclonal antibodies to GM130 (ab52649) and rabbit polyclonal antibody to SEC61β (ab15576) were purchased from Abcam. GFAP and NeuN mouse monoclonal antibodies were purchased from EMD Millipore. Mouse monoclonal antibodies to β-actin, HA, Myc, and Flag were purchased from Sigma-Aldrich. HRP-, Cy3-, and FITC-conjugated secondary antibodies were from Jackson ImmunoResearch Laboratories, Inc.

Western blotting and IP

Cells were lysed in ice-cold Triton X-100 buffer (20 mM Tris-HCl, pH 7.5, 100 mM NaCl, 1% Triton X-100, and 1 mM PMSF) or RIPA buffer (20 mM Tris-HCl pH 7.5, 100 mM NaCl, 0.1% SDS, 0.5% sodium deoxycholate, and 1 mM PMSF) containing Complete Protease Inhibitor Cocktail (Roche). Cell lysates were spun down at 12,000 rpm for 10 min, and 50 µg supernatants were resolved on SDS-PAGE and blotted with the indicated antibodies. The amount of β-actin was used as the loading control. Blots were developed with an ECL Select Western Blotting Detection system (GE Healthcare) and imaged with the Minichemi machine (Sagecreation). Quantification of Western blots was performed using ImageJ software.

To test the direct interaction of two proteins tagged with different epitopes, the corresponding expression vectors were cotransfected in HEK293 cells. 48 h later, cells were lysed in regular IP buffer (20 mM Tris-HCl, pH 7.5, 100 mM NaCl, 1% NP-40, 1 mM PMSF, and 1% glycerol) containing Complete Protease Inhibitor Cocktail. Cell lysates were spun at 12,000 rpm for 10 min at 4°C, and the supernatants were incubated with Flag antibody (M2)–conjugated or HA antibody–conjugated beads (~5 µg antibody for each sample) overnight at 4°C. The beads were centrifuged and washed three times with IP buffer. Precipitated proteins were resolved by SDS-PAGE, blotted, and probed with different antibodies.

Immunostaining and confocal microscopy

Cells grown on coverslips were fixed for 15 min at RT in 4% PFA followed by permeabilization for 10 min at RT with 0.05% saponin. After extensive washing with PBS, cells were incubated with primary antibodies in PBS containing 5% BSA at 4°C overnight. Cells were washed extensively again and incubated with secondary antibodies for 1 h at RT. After another round of thorough washing, cells were mounted with VECTASHIELD (H-1500; Vector Laboratories) and sealed on slides for microscopy analysis. For live-cell imaging, cells were grown in confocal dishes (Glass Bottom Dish; In Vitro Scientific). Samples were examined with an inverted FV1000 confocal microscope system (IX81; Olympus) using a 60× 1.42-NA oil objective. Excitation was achieved using gas-state 488-nm and solid-state 595-nm lasers. All images were taken at RT and analyzed with FV10-ASW 4.0a Viewer.

TEM

Cell monolayers were fixed for 2 h at 4°C with 0.1 M PBS containing 2.5% glutaraldehyde. Fixed samples were rinsed with PBS and further fixed with 1% OsO_4 for 0.5 h at 4°C. The samples were rinsed with distilled water and dehydrated by sequential incubation with an acetone series (30%, 50%, 70%, 80%, 90%, 95%, 100%, and 100%, 5 min each). Samples were infiltrated with Araldite 502/Embed 812 by gradually increasing the concentration of acetone (25% and 50%, 20 min; 75%, 30 min; 100%, 20 h) and then polymerized at 60°C for 72 h. Embedded samples were sectioned using an UC6 ultramicrotome (Leica Biosystems) equipped with a 45° diamond knife (Diatome) to obtain 70-nm ultrathin sections. The grids were stained at RT with 2% aqueous uranyl acetate (10 min) and Reynolds lead citrate (5 min) before imaging. Imaging was performed at 80 kV on a JEM-1400 (JEOL) transmission electron microscope.

Expression vectors

Mammalian and bacterial expression vectors were constructed using standard protocols and are listed in Table S1. The following vectors were provided by other scientists: pCMV-GFP-p62, pCMV-GFP-NBR1, and pCMV-HA-p62 (Y. Chen, Tsinghua University, Beijing, China); pCMV-Myc-Ub, pET28a-Ub(K63) (K63 only) and pET28a-Ub(K48) (K48 only; W. Li, Institute of Zoology, Chinese Academy of Sciences, Beijing, China); and pcDNA3.1-Htt97Q-GFP (X. Li, Institute of Genetics and Developmental Biology, Chinese Academy of Sciences, Beijing, China).

Recombinant proteins and GST pull-down

Recombinant GST, GST-p62, GST-p62(PB1), and GST-LC3C were expressed in *Escherichia coli* BL21 (DE3) cells and purified with glutathione-Sepharose beads (GE Healthcare) according to the instructions provided by the supplier. For GST pull-down of proteins expressed in mammalian cells, cell lysates containing Flag-tagged WDR81 proteins was prepared with Triton X-100 buffer (20 mM Tris-HCl, pH 7.5, 100 mM NaCl, 1% Triton X-100, and 1 mM PMSF) as described in the Western blotting and IP section. ^{35}S-labeled WDR81 and WDR81(1–650) proteins were prepared by in vitro translation following the protocol provided by the supplier (Promega). Purified GST, GST-p62, GST-p62(PB1), or GST-LC3C proteins (5 µg each) immobilized on glutathione-Sepharose beads were incubated with cell lysates containing WDR81 or ^{35}S-labeled WDR81 or ^{35}S-labeled WDR81(1–650) proteins at 4°C overnight and then washed extensively with the same buffer. Bound proteins were resolved by SDS-PAGE and visualized by Western blot and autoradiography.

siRNAs

RNA oligos used for siRNA are listed in Table S2. Cells were transfected with 100 pmol siRNA oligos twice at an interval of 24 h using Lipofectamine 2000. Cells were subjected to further analysis 24 h after the last transfection.

positive or negative for ubiquitin (right). 30 sections from four mice for each genotype were examined. Data (mean ± SEM) were analyzed using ANOVA. ***, P < 0.001. For views of whole-brain sections in D, F, and H, multiple images (10x) were stitched together to generate the composite images. (F) p62 immunostaining and DAPI labeling in brain sections from *WDR81*$^{f/f}$ and *WDR81*$^{f/f}$*:Nestin-Cre* mice at embryonic day 14.5 (left) and 18.5 (right). The indicated cortex regions, F1, F2, F3, and F4, in each image of whole-brain sections (10× objective, top rows) were observed under a 60× objective and are shown in the middle columns (bars, 10 µm). Magnifications (4×) of the boxed regions in F1, F2, F3, and F4 are shown in the right columns (bars, 5 µm). (G) Quantification of p62 foci in brain sections shown in F. 10 sections from two mice were examined for each genotype at each embryonic stage. Data (mean ± SEM) were analyzed using ANOVA. ***, P < 0.001. (H) p62 immunostaining and DAPI labeling in lateral brain sections from *WDR81*$^{f/f}$ and *WDR81*$^{f/f}$ cKO mice at P180 (left). Boxed regions in the whole brain sections (top) were observed under 60× objective and are shown in the bottom row (bars, 10 µm). H1 and H3 indicate cortex regions. H2 and H4 indicate striatum regions. Right: >500 cells in 10 sections from two mice for each genotype were examined for p62 foci, and data (mean ± SEM) were analyzed using ANOVA. ***, P < 0.001.

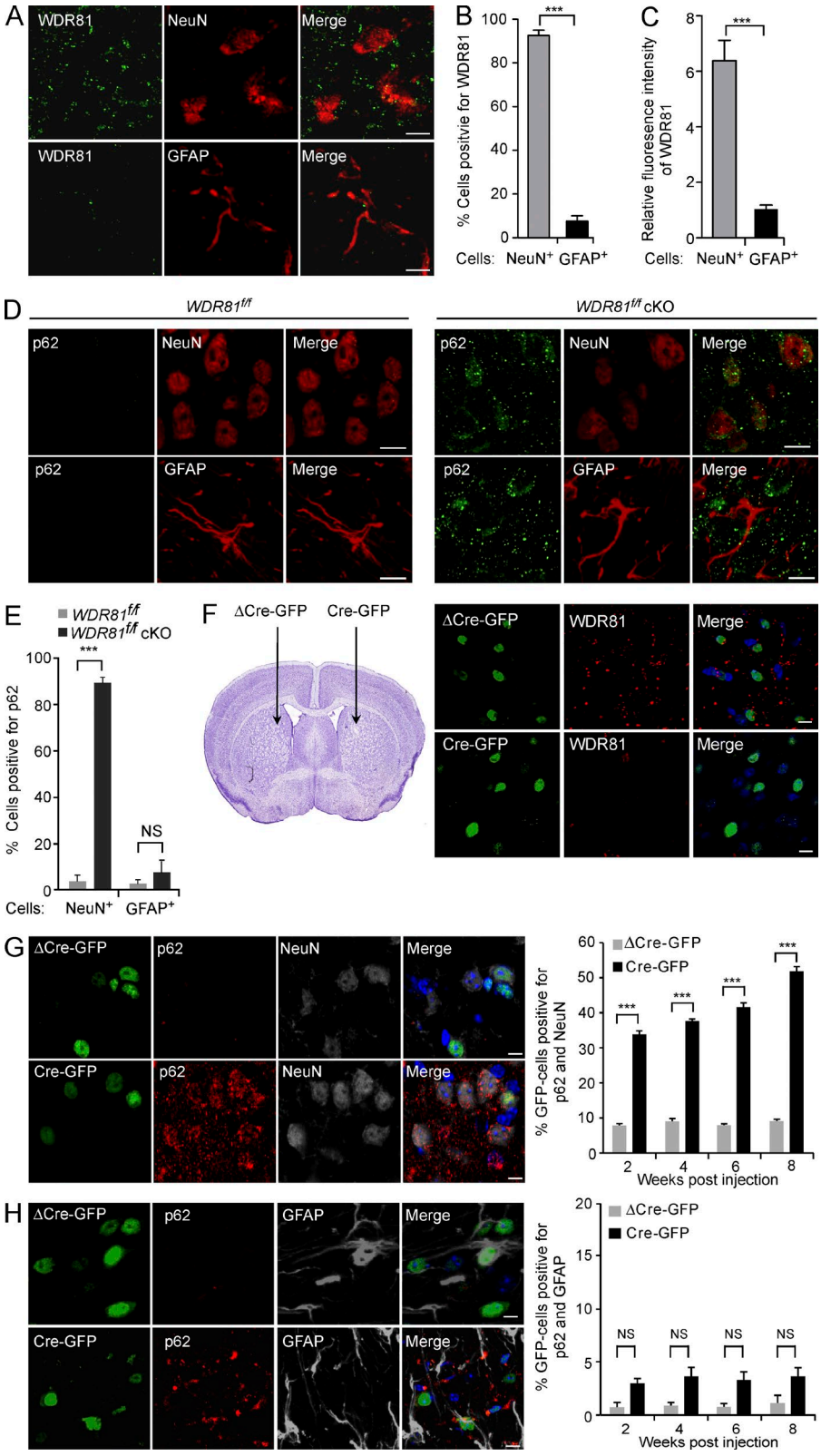

Figure 9. **WDR81 is essential for preventing accumulation of p62 foci in neuron cells in mouse brain.** (A–C) Immunohistological costaining of WDR81 with NeuN or GFAP in the mouse brain (A). Bars, 10 µm. Quantification of WDR81 expression and intensity in NeuN+ or GFAP+ cells is shown in B and C. 25 sections from three mice were examined. (D and E) Immunostaining (D) and quantification (E) of p62 and NeuN or GFAP in brain sections from *WDR81*$^{f/f}$ (top) and *WDR81*$^{f/f}$ cKO (bottom) mice at postnatal day 180. Bars, 10 µm. More than 500 cells in 10 sections from two mice for each genotype were examined for p62 foci. (F) Representative images of WDR81 and DAPI staining in brain cells infected with lentivirus expressing ΔCre-GFP or Cre-GFP (left). Bars, 10 µm. Graphic depiction of lentivirus grafting (right). Lentiviruses expressing ΔCre-GFP or Cre-GFP were grafted into contralateral sides of the same animals. (G and H) Immunostaining (left) and quantification (right) of p62 and NeuN (G) or GFAP (H) in brain sections from *WDR81*$^{f/f}$ mice infected by lentivirus expressing ΔCre-GFP or Cre-GFP. The merged images also include DAPI staining. Bars, 10 µm. >300 cells in 16 sections from four mice were examined for each treatment. For all quantifications, data (mean ± SEM) were analyzed using ANOVA, except for data in B and C (*t* test). **, P < 0.01; ***, P < 0.001; NS, not significant.

Quantitative RT-PCR

Total RNA was extracted using Trizol (Invitrogen) and chloroform. 2 µg RNA was used as template to generate cDNAs using the ImProm-II Reverse Transcription system (Promega). Quantitative RT-PCR reactions were performed on an MX3000P system (Agilent Technologies).

Generation of cell lines stably expressing Tet-on Htt97Q-GFP

HeLa cells stably expressing pcDNA6/TR (provided by Q. Chen, Institute of Zoology, Chinese Academy of Sciences, Beijing, China) were transfected with pcDNA4-Htt97Q-GFP. 24 h later, cells were subjected to selection for 2–3 wk in medium supplemented with blasticidin (5 µg/ml) and zeocin (100 µg/ml). Single colonies were picked and propagated

further. The expression of Htt97Q-GFP was induced by adding doxycycline (1 µg/ml) and observed by fluorescence microscopy.

Htt polyQ clearance assay

HeLa cells stably expressing Tet-on Htt97Q-GFP were transfected twice at an interval of 24 h with siRNA oligos for individual autophagy factors. 12 h after the second siRNA transfection, Htt97Q-GFP expression was induced with 1 µg/ml doxycycline. The medium was changed 12 h later to remove the doxycycline, and the cells were split into several dishes for the remaining siRNA treatments. Time-course quantification of polyQ foci was performed 12 h after the induction of Htt97Q-GFP expression.

Site-directed mutagenesis

WDR81 and LC3C mutants were generated by PCR-mediated mutagenesis with pairs of oligos listed in Table S3.

In vitro PI3K complex activity assay

HeLa cells of different genotype were harvested and lysed with lysis buffer (50 mM Tris-HCl, pH 7.4, 150 mM NaCl, 1% Triton X-100, and protease inhibitor cocktail). Endogenous Vps34 was immunoprecipitated by antibody against Beclin1 and Atg14L (Medical & Biological Laboratories). Immunoprecipitated beads were extensively washed with lysis buffer and further washed twice with reaction buffer (40 mM Tris-HCl, pH 7.5, 20 mM $MgCl_2$, and 1 mg/ml BSA). The beads were then incubated with 10 µg sonicated phosphatidylinositol (Sigma-Aldrich) and 1 µl 10 mM ATP in 30 µl reaction buffer for 30 min at RT. Conversion of ATP to ADP was measured with an ADP-GloTM kinase assay kit (Promega) following the instructions provided by the manufacturer.

Mice

WDR81$^{f/f}$ mice were generated by BIOCYTOGEN. *WDR81*$^{f/f}$ and *Nestin-Cre* mice were bred onto the C57B/L6 background and housed at the animal facility at the Institute of Genetics and Developmental Biology, Chinese Academy of Sciences. All procedures and husbandry were performed according to protocols approved by the Institutional Animal Care and Use Committee at Institute of Genetics and Developmental Biology.

Paraffin-embedded embryonic mouse brain sections

Freshly dissected brains were fixed with 4% PFA for 24–48 h at 4°C, then dehydrated by sequential washes in graded ethanols (70%, 80%, and 95%, 45 min each, followed by 100% alcohol, 1 h, three times). Brains were cleared in xylene for 1 h with two repeats and then immersed in paraffin for 1 h with three repeats. The brains were embedded in a paraffin block. Sections (8 µm thickness) were generated on a microtome and floated in a water bath at 40°C. The sections were transferred onto glass slides and deparaffinized twice in xylene (5 min each). The slides were then rehydrated by sequential washes in graded ethanols (100%, 100%, 95%, 85%, 70%, and 50%, each for 3 min) at room temperature. After a final wash in 0.85% NaCl for 5 min at room temperature, the slides were subjected to immunohistological analysis.

Immunohistology

Mice were euthanized by intraperitoneal injection of Avertin (50× stock solution: 10 g tribromoethanol [Thermo Fisher Scientific] in 10 ml tert-amyl alcohol [Sigma-Aldrich]), then transcardially perfused with saline followed by 4% PFA. Brains were dissected out, postfixed overnight in 4% PFA, and then equilibrated in 30% sucrose. Brain sections (40 µm thickness) were generated using a sliding microtome and stored in a −20°C freezer as floating sections in 96-well plates filled with cryoprotectant solution (glycerol, ethylene glycol, and 0.1 M phosphate buffer, pH 7.4, 1:1:2 by volume).

For immunohistological analysis, brain sections were washed extensively with TBS (50 mM Tris-HCl, pH 7.2, and 100 mM NaCl) and blocked with 5% donkey serum containing 0.05% Triton X-100 for 1 h at room temperature. Brain sections were then incubated with primary antibodies in TBS containing 5% donkey serum at 4°C overnight. After extensive washing, the sections were incubated with secondary antibodies for 1 h at room temperature. After staining, sections were mounted, coverslipped, and maintained at 4°C in the dark until analysis.

Recombinant lentivirus and in vivo lentiviral grafting

Lentivirus production and lentiviral grafting were performed as described previously (Guo et al., 2011b). In brief, lentiviral transfer vector DNA and packaging plasmid DNA were cotransfected into 293T cells. The medium was collected and pooled at 40, 64, and 88 h and then filtered through a 0.2-µm filter. Viruses were concentrated by ultracentrifugation at 19,000 rpm for 2 h at 20°C using a SW27 rotor (Beckman Coulter). To determine the titer of the viruses, the virus preparation was made in 10-fold serial dilutions. 2 µl of each dilution was used to infect 100,000 HeLa cells/well in six-well plates. 48 h later, cells were collected and analyzed by flow cytometry. The percentage of GFP-positive cells between 1% and 10% was used to calculate virus titer (infection units per microliter) using the following formula: titer (infection units per microliter) = [(percentage of GFP-positive cells) × 100,000 × dilution factor]/2. For in vivo lentiviral grafting, 4-wk-old C57B/L6 male mice were anesthetized, and viruses ($\geq 10^8$ viruses/µl in 1.5 µl) were injected stereotaxically into the striatum using the following coordinates relative to bregma: anteroposterior, 0 mm; lateral, ±2 mm; ventral, −2 mm (from dura). Every 2 weeks after viral grafting, mice were deeply anesthetized with avertin and perfused with saline followed by 4% PFA.

Statistical analysis

Data were analyzed with Prism (GraphPad Software) to generate bar graphs. Error bars represent SEM. The two-tailed unpaired *t* test was used for statistical comparisons of two groups of samples. Analysis of variance (ANOVA) with a Newman–Keuls posttest was used for statistical comparisons of multiple groups of samples. $P > 0.05$ was considered not significant.

Online supplemental material

Fig. S1 describes the subcellular localization of WDR81. Fig. S2 shows that WDR81 is important for clearance of polyQ aggregates, but not essential for general autophagy. Fig. S3 demonstrates that WDR91 is not required in aggrephagy. Fig. S4 shows that WDR81 is recruited by p62, but not other autophagy receptors or adaptors. Fig. S5 characterizes the recruitment of major autophagy regulators to Ub foci, the expression of LC3C in different cell types and mouse brain, the WDR81 LIR motifs, and the interaction of p62 with LC3C mutants. Table S1 summarizes the mammalian expression vectors used in the study. Table S2 lists oligos used for siRNA. Table S3 lists oligos used for site-directed mutagenesis.

Acknowledgments

We thank Drs. H. Zhang, X.C. Wang, L. Yu, Y.G. Chen, Q. Chen, W. Li, and X.J. Li for expression vectors and Drs. E. White, N. Mizushima, and L. Yu for p62, ATG5, and ATG12 knockout cell lines.

This research was supported by the National Basic Research Program of China (grant 2013CB910102), the National Science Foundation of China (grant 31230043 to C. Yang and grant 31428014 to S. Luo), the Chinese Academy of Sciences Interdisciplin-

ary Innovation Team (C. Yang), and the Chinese Academy of Sciences Key Research Program of Frontier Sciences (grant QYZDB-SSW-SMC046 to W. Guo). W. Guo was funded by the Recruitment Program of the Global Youth Experts of China, 2015.

The authors declare no competing financial interests.

Author contributions: C. Yang, X. Liu, Y. Li, and W. Guo conceived and designed the research. X. Liu, Y. Li, and W. Gou performed most of the biochemical, cell biology, and animal experiments. X. Wang performed TEM analysis. K. Liu, Q. Gan, Z. Gao, and Y. Jian generated some antibodies and plasmids. X. Liu, Y. Li, S. Luo, W. Guo, and C. Yang analyzed and interpreted the experimental data. C. Yang, X. Liu, Y. Li, and W. Guo wrote the paper, and all authors commented on the manuscript.

Submitted: 11 August 2016
Revised: 23 December 2016
Accepted: 2 March 2017

References

Bjørkøy, G., T. Lamark, A. Brech, H. Outzen, M. Perander, A. Overvatn, H. Stenmark, and T. Johansen. 2005. p62/SQSTM1 forms protein aggregates degraded by autophagy and has a protective effect on huntingtin-induced cell death. *J. Cell Biol.* 171:603–614. http://dx.doi.org/10.1083/jcb.200507002

Blobel, G. 1971. Release, identification, and isolation of messenger RNA from mammalian ribosomes. *Proc. Natl. Acad. Sci. USA*. 68:832–835. http://dx.doi.org/10.1073/pnas.68.4.832

Clausen, T.H., T. Lamark, P. Isakson, K. Finley, K.B. Larsen, A. Brech, A. Øvervatn, H. Stenmark, G. Bjørkøy, A. Simonsen, and T. Johansen. 2010. p62/SQSTM1 and ALFY interact to facilitate the formation of p62 bodies/ALIS and their degradation by autophagy. *Autophagy.* 6:330–344. http://dx.doi.org/10.4161/auto.6.3.11226

Cullinane, A.R., A.A. Schäffer, and M. Huizing. 2013. The BEACH is hot: A LYST of emerging roles for BEACH-domain containing proteins in human disease. *Traffic.* 14:749–766. http://dx.doi.org/10.1111/tra.12069

Filimonenko, M., S. Stuffers, C. Raiborg, A. Yamamoto, L. Malerød, E.M. Fisher, A. Isaacs, A. Brech, H. Stenmark, and A. Simonsen. 2007. Functional multivesicular bodies are required for autophagic clearance of protein aggregates associated with neurodegenerative disease. *J. Cell Biol.* 179:485–500. http://dx.doi.org/10.1083/jcb.200702115

Filimonenko, M., P. Isakson, K.D. Finley, M. Anderson, H. Jeong, T.J. Melia, B.J. Bartlett, K.M. Myers, H.C. Birkeland, T. Lamark, et al. 2010. The selective macroautophagic degradation of aggregated proteins requires the PI3P-binding protein Alfy. *Mol. Cell.* 38:265–279. http://dx.doi.org/10.1016/j.molcel.2010.04.007

Gamerdinger, M., P. Hajieva, A.M. Kaya, U. Wolfrum, F.U. Hartl, and C. Behl. 2009. Protein quality control during aging involves recruitment of the macroautophagy pathway by BAG3. *EMBO J.* 28:889–901. http://dx.doi.org/10.1038/emboj.2009.29

Goldberg, A.L. 2003. Protein degradation and protection against misfolded or damaged proteins. *Nature.* 426:895–899. http://dx.doi.org/10.1038/nature02263

Gulsuner, S., A.B. Tekinay, K. Doerschner, H. Boyaci, K. Bilguvar, H. Unal, A. Ors, O.E. Onat, E. Atalar, A.N. Basak, et al. 2011. Homozygosity mapping and targeted genomic sequencing reveal the gene responsible for cerebellar hypoplasia and quadrupedal locomotion in a consanguineous kindred. *Genome Res.* 21:1995–2003. http://dx.doi.org/10.1101/gr.126110.111

Guo, J.Y., H.Y. Chen, R. Mathew, J. Fan, A.M. Strohecker, G. Karsli-Uzunbas, J.J. Kamphorst, G. Chen, J.M. Lemons, V. Karantza, et al. 2011a. Activated Ras requires autophagy to maintain oxidative metabolism and tumorigenesis. *Genes Dev.* 25:460–470. http://dx.doi.org/10.1101/gad.2016311

Guo, W., L. Zhang, D.M. Christopher, Z.Q. Teng, S.R. Fausett, C. Liu, O.L. George, J. Klingensmith, P. Jin, and X. Zhao. 2011b. RNA-binding protein FXR2 regulates adult hippocampal neurogenesis by reducing Noggin expression. *Neuron.* 70:924–938. http://dx.doi.org/10.1016/j.neuron.2011.03.027

Haigh, J.J., P.I. Morelli, H. Gerhardt, K. Haigh, J. Tsien, A. Damert, L. Miquerol, U. Muhlner, R. Klein, N. Ferrara, et al. 2003. Cortical and retinal defects caused by dosage-dependent reductions in VEGF-A paracrine signaling. *Dev. Biol.* 262:225–241. http://dx.doi.org/10.1016/S0012-1606(03)00356-7

Johansen, T., and T. Lamark. 2011. Selective autophagy mediated by autophagic adapter proteins. *Autophagy.* 7:279–296. http://dx.doi.org/10.4161/auto.7.3.14487

Kawaguchi, Y., J.J. Kovacs, A. McLaurin, J.M. Vance, A. Ito, and T.P. Yao. 2003. The deacetylase HDAC6 regulates aggresome formation and cell viability in response to misfolded protein stress. *Cell.* 115:727–738. http://dx.doi.org/10.1016/S0092-8674(03)00939-5

Khaminets, A., C. Behl, and I. Dikic. 2016. Ubiquitin-dependent and independent signals in selective autophagy. *Trends Cell Biol.* 26:6–16. http://dx.doi.org/10.1016/j.tcb.2015.08.010

Kirkin, V., T. Lamark, Y.S. Sou, G. Bjørkøy, J.L. Nunn, J.A. Bruun, E. Shvets, D.G. McEwan, T.H. Clausen, P. Wild, et al. 2009a. A role for NBR1 in autophagosomal degradation of ubiquitinated substrates. *Mol. Cell.* 33:505–516. http://dx.doi.org/10.1016/j.molcel.2009.01.020

Kirkin, V., D.G. McEwan, I. Novak, and I. Dikic. 2009b. A role for ubiquitin in selective autophagy. *Mol. Cell.* 34:259–269. http://dx.doi.org/10.1016/j.molcel.2009.04.026

Komatsu, M., S. Waguri, M. Koike, Y.S. Sou, T. Ueno, T. Hara, N. Mizushima, J. Iwata, J. Ezaki, S. Murata, et al. 2007. Homeostatic levels of p62 control cytoplasmic inclusion body formation in autophagy-deficient mice. *Cell.* 131:1149–1163. http://dx.doi.org/10.1016/j.cell.2007.10.035

Kopito, R.R. 2000. Aggresomes, inclusion bodies and protein aggregation. *Trends Cell Biol.* 10:524–530. http://dx.doi.org/10.1016/S0962-8924(00)01852-3

Kuma, A., M. Hatano, M. Matsui, A. Yamamoto, H. Nakaya, T. Yoshimori, Y. Ohsumi, T. Tokuhisa, and N. Mizushima. 2004. The role of autophagy during the early neonatal starvation period. *Nature.* 432:1032–1036. http://dx.doi.org/10.1038/nature03029

Lazarou, M., D.A. Sliter, L.A. Kane, S.A. Sarraf, C. Wang, J.L. Burman, D.P. Sideris, A.I. Fogel, and R.J. Youle. 2015. The ubiquitin kinase PINK1 recruits autophagy receptors to induce mitophagy. *Nature.* 524:309–314. http://dx.doi.org/10.1038/nature14893

Lim, J., M.L. Lachenmayer, S. Wu, W. Liu, M. Kundu, R. Wang, M. Komatsu, Y.J. Oh, Y. Zhao, and Z. Yue. 2015. Proteotoxic stress induces phosphorylation of p62/SQSTM1 by ULK1 to regulate selective autophagic clearance of protein aggregates. *PLoS Genet.* 11:e1004987. http://dx.doi.org/10.1371/journal.pgen.1004987

Lin, L., P. Yang, X. Huang, H. Zhang, Q. Lu, and H. Zhang. 2013. The scaffold protein EPG-7 links cargo-receptor complexes with the autophagic assembly machinery. *J. Cell Biol.* 201:113–129. http://dx.doi.org/10.1083/jcb.201209098

Liu, K., Y. Jian, X. Sun, C. Yang, Z. Gao, Z. Zhang, X. Liu, Y. Li, J. Xu, Y. Jing, et al. 2016. Negative regulation of phosphatidylinositol 3-phosphate levels in early-to-late endosome conversion. *J. Cell Biol.* 212:181–198. (published erratum appears in *J. Cell Biol.* 2016. 212:739). http://dx.doi.org/10.1083/jcb.201506081

Liu, L., D. Feng, G. Chen, M. Chen, Q. Zheng, P. Song, Q. Ma, C. Zhu, R. Wang, W. Qi, et al. 2012. Mitochondrial outer-membrane protein FUNDC1 mediates hypoxia-induced mitophagy in mammalian cells. *Nat. Cell Biol.* 14:177–185. http://dx.doi.org/10.1038/ncb2422

Lystad, A.H., Y. Ichimura, K. Takagi, Y. Yang, S. Pankiv, Y. Kanegae, S. Kageyama, M. Suzuki, I. Saito, T. Mizushima, et al. 2014. Structural determinants in GABARAP required for the selective binding and recruitment of ALFY to LC3B-positive structures. *EMBO Rep.* 15:557–565. http://dx.doi.org/10.1002/embr.201338003

Matsumoto, G., K. Wada, M. Okuno, M. Kurosawa, and N. Nukina. 2011. Serine 403 phosphorylation of p62/SQSTM1 regulates selective autophagic clearance of ubiquitinated proteins. *Mol. Cell.* 44:279–289. http://dx.doi.org/10.1016/j.molcel.2011.07.039

Menzies, F.M., A. Fleming, and D.C. Rubinsztein. 2015. Compromised autophagy and neurodegenerative diseases. *Nat. Rev. Neurosci.* 16:345–357. http://dx.doi.org/10.1038/nrn3961

Moscat, J., and M.T. Diaz-Meco. 2009. p62 at the crossroads of autophagy, apoptosis, and cancer. *Cell.* 137:1001–1004. http://dx.doi.org/10.1016/j.cell.2009.05.023

Newton, K., M.L. Matsumoto, I.E. Wertz, D.S. Kirkpatrick, J.R. Lill, J. Tan, D. Dugger, N. Gordon, S.S. Sidhu, F.A. Fellouse, et al. 2008. Ubiquitin chain editing revealed by polyubiquitin linkage-specific antibodies. *Cell.* 134:668–678. http://dx.doi.org/10.1016/j.cell.2008.07.039

Noda, N.N., Y. Ohsumi, and F. Inagaki. 2010. Atg8-family interacting motif crucial for selective autophagy. *FEBS Lett.* 584:1379–1385. http://dx.doi.org/10.1016/j.febslet.2010.01.018

Pankiv, S., T.H. Clausen, T. Lamark, A. Brech, J.A. Bruun, H. Outzen, A. Øvervatn, G. Bjørkøy, and T. Johansen. 2007. p62/SQSTM1 binds directly to Atg8/LC3 to facilitate degradation of ubiquitinated protein aggregates by autophagy. *J. Biol. Chem.* 282:24131–24145. http://dx.doi.org/10.1074/jbc.M702824200

Rapiteanu, R., L.J. Davis, J.C. Williamson, R.T. Timms, J. Paul Luzio, and P.J. Lehner. 2016. A genetic screen identifies a critical role for the WDR81-WDR91 complex in the trafficking and degradation of tetherin. *Traffic.* 17:940–958. http://dx.doi.org/10.1111/tra.12409

Rogov, V., V. Dötsch, T. Johansen, and V. Kirkin. 2014. Interactions between autophagy receptors and ubiquitin-like proteins form the molecular basis for selective autophagy. *Mol. Cell.* 53:167–178. http://dx.doi.org/10.1016/j.molcel.2013.12.014

Rubinsztein, D.C. 2006. The roles of intracellular protein-degradation pathways in neurodegeneration. *Nature.* 443:780–786. http://dx.doi.org/10.1038/nature05291

Rui, Y.N., Z. Xu, B. Patel, Z. Chen, D. Chen, A. Tito, G. David, Y. Sun, E.F. Stimming, H.J. Bellen, et al. 2015. Huntingtin functions as a scaffold for selective macroautophagy. *Nat. Cell Biol.* 17:262–275. http://dx.doi.org/10.1038/ncb3101

Salomons, F.A., V. Menéndez-Benito, C. Böttcher, B.A. McCray, J.P. Taylor, and N.P. Dantuma. 2009. Selective accumulation of aggregation-prone proteasome substrates in response to proteotoxic stress. *Mol. Cell. Biol.* 29:1774–1785. http://dx.doi.org/10.1128/MCB.01485-08

Seibenhener, M.L., J.R. Babu, T. Geetha, H.C. Wong, N.R. Krishna, and M.W. Wooten. 2004. Sequestosome 1/p62 is a polyubiquitin chain binding protein involved in ubiquitin proteasome degradation. *Mol. Cell. Biol.* 24:8055–8068. http://dx.doi.org/10.1128/MCB.24.18.8055-8068.2004

Szeto, J., N.A. Kaniuk, V. Canadien, R. Nisman, N. Mizushima, T. Yoshimori, D.P. Bazett-Jones, and J.H. Brumell. 2006. ALIS are stress-induced protein storage compartments for substrates of the proteasome and autophagy. *Autophagy.* 2:189–199. http://dx.doi.org/10.4161/auto.2731

Tan, J.M., E.S. Wong, D.S. Kirkpatrick, O. Pletnikova, H.S. Ko, S.P. Tay, M.W. Ho, J. Troncoso, S.P. Gygi, M.K. Lee, et al. 2008. Lysine 63-linked ubiquitination promotes the formation and autophagic clearance of protein inclusions associated with neurodegenerative diseases. *Hum. Mol. Genet.* 17:431–439. http://dx.doi.org/10.1093/hmg/ddm320

Traka, M., K.J. Millen, D. Collins, B. Elbaz, G.J. Kidd, C.M. Gomez, and B. Popko. 2013. WDR81 is necessary for purkinje and photoreceptor cell survival. *J. Neurosci.* 33:6834–6844. http://dx.doi.org/10.1523/JNEUROSCI.2394-12.2013

Tyedmers, J., A. Mogk, and B. Bukau. 2010. Cellular strategies for controlling protein aggregation. *Nat. Rev. Mol. Cell Biol.* 11:777–788. http://dx.doi.org/10.1038/nrm2993

von Muhlinen, N., M. Akutsu, B.J. Ravenhill, Á. Foeglein, S. Bloor, T.J. Rutherford, S.M.V. Freund, D. Komander, and F. Randow. 2012. LC3C, bound selectively by a noncanonical LIR motif in NDP52, is required for antibacterial autophagy. *Mol. Cell.* 48:329–342. http://dx.doi.org/10.1016/j.molcel.2012.08.024

Wild, P., H. Farhan, D.G. McEwan, S. Wagner, V.V. Rogov, N.R. Brady, B. Richter, J. Korac, O. Waidmann, C. Choudhary, et al. 2011. Phosphorylation of the autophagy receptor optineurin restricts *Salmonella* growth. *Science.* 333:228–233. http://dx.doi.org/10.1126/science.1205405

Wong, E., and A.M. Cuervo. 2010. Autophagy gone awry in neurodegenerative diseases. *Nat. Neurosci.* 13:805–811. http://dx.doi.org/10.1038/nn.2575

Wu, F., Y. Watanabe, X.Y. Guo, X. Qi, P. Wang, H.Y. Zhao, Z. Wang, Y. Fujioka, H. Zhang, J.Q. Ren, et al. 2015. Structural basis of the differential function of the two *C. elegans* Atg8 homologs, LGG-1 and LGG-2, in autophagy. *Mol. Cell.* 60:914–929. http://dx.doi.org/10.1016/j.molcel.2015.11.019